Phase transitions of fluids in shear flow

1997 J. Phys.: Condens. Matter 9 6119

(http://iopscience.iop.org/0953-8984/9/29/001)

J. Phys.: Condens. Matter **9** (1997) 6119–6157. Printed in the UK PII: S0953-8984(97)66281-5

REVIEW ARTICLE

Phase transitions of fluids in shear flow

Akira Onuki
Department of Physics, Kyoto University, Kyoto 606, Japan

Received 14 March 1997

Abstract. We review theories and experiments on the effects of shear in fluids undergoing phase transitions. We put emphasis on near-critical fluids and polymer solutions as representative examples, but also discuss related problems in polymer blends, gels, and surfactant systems, etc. In near-critical fluids, convective deformations can drastically alter the critical behaviour, spinodal decomposition, and nucleation. In this case the hydrodynamic interaction suppresses the fluctuations and gives rise to a downward shift of the critical temperature (shear-induced mixing). The rheology in two-phase states, and effects of random stirring are also reviewed. In semidilute polymer solutions near the coexistence curve, on the other hand, the composition fluctuations can be strongly influenced by the viscoelastic stress. In shear flow, this dynamical coupling results in enhancement of the composition fluctuations (shear-induced demixing). They grow, but are eventually disrupted by convective deformations, yielding chaotic dynamical steady states where phase separation is incompletely taking place. Such nonlinear shear regimes are examined using computer simulations based on a viscoelastic Ginzburg–Landau model.

Contents

1. Introduction

Flows of fluids are described by a space-time-dependent velocity field. In contrast to solids, fluids do not return to their original forms after experiencing shear deformation. The simplest example is a plane shear flow whose average profile is

$$\langle \boldsymbol{v} \rangle = Sy\boldsymbol{e}_x \tag{1.1}$$

0953-8984/97/296119+39$19.50

with a spatially homogeneous shear rate S. Hereafter the flow direction is taken to be along the x-axis, $\boldsymbol{e}_x$ being the unit vector along the x-axis, and the mean velocity varies in the y- or shear direction, while the z-direction is called the vorticity direction. As is well known, if a fixed shear is applied to a fluid of viscosity η, a shear stress $\sigma_{xy} = \eta S$ arises. In this typical example of nonequilibrium steady states, the size of S is mostly assumed to be much smaller than any underlying relaxation times of the fluid. This is the necessary condition for justifying the usual hydrodynamic theory on the basis of the local equilibrium approximation. However, in recent years, much attention has come to be focused on nonlinear cases, in which a certain internal structure of the fluid is strongly affected by the flow field [1–3]. Particularly striking effects arise when shear influences phase transitions and phase separation of fluids. Though such effects have been known of in polymer science, without satisfactory explanations [4–8], they are becoming very important in the study of fluids near the critical point (near-critical fluids) and various complex fluids such as polymers, liquid crystals, colloidal systems, and amphiphilic systems. This trend has developed out of the foundation of a deep understanding of dynamical critical phenomena [9, 10], kinetics of first-order phase transitions [11, 12], and polymer physics [13, 14]. Experimentally, this investigation has been accelerated through the recent application of scattering techniques to nonequilibrium phenomena under shear. Other optical effects such as birefringence and dichroism have also been useful for sensitively detecting spatial anisotropy of composition fluctuations, and molecular alignment (see the last paragraph of this section). The information gained by these means can then be combined with rheological data on the shear stress and normal-stress differences, which in many cases exhibit unusual behaviour in nonlinear-response regimes of shear. Though the study of complex fluids under shear has often been conducted with the goal of producing engineering-oriented results, it is now developing into a new interdisciplinary field, between engineering and physics. Here, rheology and phase transitions are closely and uniquely tied.

Cases in which shear effects are particularly striking and well known include the following.

(1) *Fluids with slowly relaxing fluctuations*. A representative example here is a fluid near its critical point, in which the critical fluctuations are greatly deformed as they are convected by a spatially varying velocity field [15–19]. The deformation time is given by the inverse shear $1/S$, so the deformation is strong or nonlinear when the so-called Deborach number De defined by

$$De = S\tau_\xi \tag{1.2}$$

exceeds 1 (the strong-shear case), where τ_ξ is the characteristic lifetime of the critical fluctuations on the spatial scale of the correlation length ξ and can be measured by means of dynamical light scattering. As other conspicuous examples, even not close to critical points, entangled polymers [13, 14] and colloidal systems [20–22] exhibit slow stress and density relaxations, and are easily driven into nonlinear-response regimes of shear.

(2) *Phase-separating fluids*. In a thermodynamically unstable or metastable fluid, two-phase structures emerge after quenching a fluid. The domain size is small initially and grows in time, so the driving force of the instability decreases, and shear can eventually suppress the growth, resulting in a dynamically steady, two-phase state. On the other hand, nucleation can be suppressed if droplets with the critical size R_c are unstable against break-up in shear. Furthermore, surfactant molecules, if they are added, tend to be trapped in the interface regions, and can stabilize two-phase structures, producing a number of complex and intriguing effects on the two-phase domain structure. Shear flow can drastically affect phase behaviour of such amphiphilic systems [23–26].

(3) *Viscoelastic two-component fluids.* When the two components have very different viscoelastic properties, there arises a dynamical coupling between the stress and diffusion in such systems, leading to a number of viscoelastic effects. Among them, shear-induced phase separation in semidilute polymer solutions is the most spectacular, and is one of the main subjects of this paper. In this case the composition fluctuations produce inhomogeneities of stress imbalance resulting in diffusion in the direction of phase separation, giving rise to enhanced light scattering even above the coexistence temperature [8].

(4) *Fluids composed of large (although perhaps simple) constituent elements*. In colloidal systems, even when a relatively weak experimentally producible shear is applied, the structure of the phase can be changed drastically. In particular, shear-induced melting of crystal structures has been studied by means of scattering experiments [20–22]. In order to produce the same type of change in fluids of small molecules, an unreasonably large shear must be used. Moreover, a gas–liquid critical point has recently been found in colloidal systems, in which the critical fluctuations are extremely sensitive to shear [27].

(5) *Fluids with complex internal structure and long-range order*. Examples include various mesoscopic phases of liquid crystals [28–31], block copolymers [32–36], and amphiphilic systems [23–26]. It is obvious that structures such as lamellae or cylinders are easily aligned by relatively weak shear. Even their structures and phase behaviour can be altered by shear near the transition point. For example, shear can induce transitions between phases of lamellae and monodisperse multilamellar vesciles [24] and between isotropic and nematic phases giving rise to two-phase coexistence in homogeneous flow [23, 25]. Defects can be removed or even generated by shear [37]. We also mention electro-rheological and ferromagnetic fluids, in which stringlike structures of colloidal particles are formed due to dipolar interaction under an electric or magnetic field. They exhibit unique rheology and phase behaviour in shear flow [38, 39].

There can be many other cases. Less studied in physics but important in polymer science are crystallization [40, 41] and gelation [42, 43] of polymers in a flow field. For highly viscous fluids around the glass transition, the structural relaxation time becomes exceedingly long, and a marked shear-thinning effect was observed [44]. Very recent molecular dynamics simulations on a highly supercooled liquid have reproduced such behaviour [45]. We should not forget to mention boundary effects such as the effects of slipping of a viscoelastic fluid at a solid boundary [46, 47] or plug flow formation in dense suspensions passing through a capillary [48–50]. Furthermore, application of shear to molecular systems inserted between two solid plates with spacing of the order of 10 Å has become possible. In such confined systems, measurements of the shear stress give information on the shear-induced melting of a solid phase and nonlinear rheology of a fluid phase [51, 52].

A large number of papers have thus been published on shear flow effects in various fluids undergoing some phase transition. It is not easy to cover all of these topics in a single review. This is also so because most of them are still developing and not well understood. In this article we will focus our attention mainly on near-critical fluids in the above-mentioned categories (1) and (2) in section 2, and semidilute polymer solutions in the category (3) in section 3. The theoretical foundation of near-critical fluids has no ambiguity, while that of polymer solutions has begun to be understood. We will also discuss cases of other fluids as much as possible. The approaches here can be starting points for investigating other fluids under shear.

We will thus treat bulk shear effects independent of the distance to the boundary. We are above all interested in the structure factor $I(\boldsymbol{q})$ of the composition fluctuations observable by scattering methods. Here we explain why it can be well defined in moving fluids under

shear flow (1.1), which is not trivial. That is, we show that a sheared fluid still maintains a translational invariance in spatial regions far from the boundary, which is an advantage over other nonequilibrium situations such as those under a temperature gradient. It follows from the fact that a shift of the origin of the reference frame by a along the y-axis is equivalent to a Galilean transformation to a new reference frame moving with a velocity $-aS\boldsymbol{e}_x$ [15]. This implies that, in homogeneous stationary states, the time correlation function of any density variable $\phi(\boldsymbol{r}, t)$ may be written as

$$\langle\phi(\boldsymbol{r}, t)\phi(\boldsymbol{r}', t')\rangle = \langle\phi(\boldsymbol{r} - \boldsymbol{r}' - S(t - t')y'\boldsymbol{e}_x, t - t')\phi(\boldsymbol{0}, 0)\rangle. \tag{1.3}$$

The equal-time correlation function ($t = t'$) depends only on the relative position $\boldsymbol{r} - \boldsymbol{r}'$. Its Fourier transformation yields the steady-state structure factor

$$I(\boldsymbol{q}) = \int \mathrm{d}\boldsymbol{r}\ \exp[\mathrm{i}\boldsymbol{q}\cdot(\boldsymbol{r} - \boldsymbol{r}')]\langle\phi(\boldsymbol{r}, t)\phi(\boldsymbol{r}', t)\rangle \tag{1.4}$$

which is observable by means of scattering experiments. Theoretically it goes without saying that because of the translational invariance the Fourier transformation may be used to greatly simplify the calculations. It is instructive to rewrite (1.3) in terms of the Fourier components:

$$\langle\phi_{\boldsymbol{q}}(t)\phi_{\boldsymbol{k}}(t')\rangle = (2\pi)^d\delta(\boldsymbol{q} + \boldsymbol{k} + q_x S(t - t')\boldsymbol{e}_y)I(\boldsymbol{q}, t - t') \tag{1.5}$$

where

$$I(\boldsymbol{q}, t) = \int \mathrm{d}\boldsymbol{r}\ \exp[\mathrm{i}\boldsymbol{q}\cdot\boldsymbol{r}]\langle\phi(\boldsymbol{r}, t)\phi(\boldsymbol{0}, 0)\rangle. \tag{1.6}$$

The first factor in (1.5) is the delta function in d dimensions. To understand its origin we note that a plane-wave composition fluctuation ($\propto \exp(\mathrm{i}\boldsymbol{q}\cdot\boldsymbol{r})$ at $t = 0$) with a small amplitude changes in time into a plane wave with a time-dependent wave vector given by $\tilde{\boldsymbol{q}}(t) = \boldsymbol{q} - Stq_x\boldsymbol{e}_y$ if nonlinear couplings among the fluctuations are neglected. Then (1.6) is nonvanishing only for $\tilde{\boldsymbol{q}}(-t + t') = -\boldsymbol{k}$ on average over the fluctuations, yielding the above delta function. It would be informative to measure the time dependence of $I(\boldsymbol{q}, t)$ in (1.5), but dynamical light scattering in shear flow has not yet been successful. This seems to be because the Doppler shift of scattered light depends on the y-coordinate of the scattering position, and the observed signal strongly depends on the thickness of the scattering region in the y-direction [53, 54].

We also note that anisotropic composition fluctuations in shear flow or electric field give rise to anisotropy in the average dielectric tensor at optical frequencies even when the constituent particles are optically isotropic [14, 55]. Its real and imaginary parts lead to the so-called form birefringence and dichroism, respectively. In particular, the form dichroism is significant when the spatial scales of scattering objects are comparable to the light wavelength. This effect has been measured in near-critical fluids [56] and polymeric systems [57] in shear flow. On the other hand, alignment of optically anisotropic molecules in the external field gives rise to the so-called intrinsic birefringence, whereas the intrinsic dichroism is negligible for visible light in most cases.

2. Near-critical fluids under shear

In this section we will mainly consider near-critical fluids in which the critical fluctuations are important. However, readers need not be unduly concerned with the mathematical details of the theory. We start with mean-field calculations, and take into account the renormalization effects in the simplest manner. Shear effects arise solely from

position-dependent convection or convective deformations of the composition fluctuations. Nevertheless, the effects are very complex and even surprising, particularly in spinodal decomposition and nucleation. We will also discuss the effects of stirring on the critical behaviour and phase separation of fluids, which experimentalists have been interested in but have not yet well understood.

2.1. The dynamical model

In near-critical fluids, a scalar order parameter $\psi(\boldsymbol{r}, t)$ exhibits enormous thermal fluctuations on approaching the critical point [9, 10]. We will call this the composition, supposing a fluid binary mixture near the consolute critical point with a weak singularity of the isothermal compressibility. While its local variations remain small, its spatial correlations extend over a long distance ξ, which is the origin of various critical singularities. This length is called the correlation length, and grows as $\xi = \xi_0(T/T_c - 1)^{-\nu}$ as $T \to T_c$ at the critical value of the average composition, ξ_0 being a microscopic length ($\sim$2 Å) and $\nu \cong 0.625$ being the critical exponent.

The Ginzburg–Landau–Wilson free-energy functional for ψ is written in the usual form [10]:

$$F = k_B T_c \int \mathrm{d}\boldsymbol{r} \left[\frac{1}{2} r_0 \psi^2 + \frac{1}{4} u_0 \psi^4 - h\psi + \frac{1}{2} C_0 |\boldsymbol{\nabla}\psi|^2 \right]. \tag{2.1}$$

Here r_0 is the mean-field reduced temperature, and u_0 is the nonlinear coupling coefficient. h, which corresponds to a magnetic field in Ising spin systems, almost vanishes at the critical composition above T_c and on the coexistence curve. The coefficient C_0 will be set equal to 1 because it is almost unchanged even after the renormalization. The dynamical equations for ψ and the velocity field deviation $\boldsymbol{v}$ are given by [15]

$$\frac{\partial}{\partial t}\psi = -Sy \frac{\partial \psi}{\partial x} - \boldsymbol{\nabla} \cdot (\psi \boldsymbol{v}) + (L_0/k_B T_c)\, \nabla^2 \frac{\delta F}{\delta \psi} + \theta_R \tag{2.2}$$

$$\bar{\rho}\, \frac{\partial}{\partial t}\boldsymbol{v} = -\boldsymbol{\nabla} p_1 - \psi\, \boldsymbol{\nabla} \frac{\delta F}{\delta \psi} + \eta_0\, \nabla^2 \boldsymbol{v} + \boldsymbol{\zeta}_R. \tag{2.3}$$

The mass density $\bar{\rho}$ is assumed to be a constant. It is known that slow motion of ψ is not affected by the longitudinal part of $\boldsymbol{v}$, so we are allowed to consider the transverse part only:

$$\boldsymbol{\nabla} \cdot \boldsymbol{v} = 0. \tag{2.4}$$

The pressure p_1 in (2.2) is determined to ensure this condition. θ_R and $\boldsymbol{\zeta}_R$ are Gaussian–Markovian thermal noises related to the kinetic coefficients L_0 and η_0 by

$$\langle \theta_R(\boldsymbol{r}, t)\theta_R(\boldsymbol{r}', t') \rangle = -2L_0 \nabla^2 \delta(\boldsymbol{r} - \boldsymbol{r}')\delta(t - t'). \tag{2.5}$$

$$\langle \zeta_{Ri}(\boldsymbol{r}, t)\zeta_{Rj}(\boldsymbol{r}', t') \rangle = -2k_B T \eta_0 \delta_{ij} \nabla^2 \delta(\boldsymbol{r} - \boldsymbol{r}')\delta(t - t'). \tag{2.6}$$

Furthermore, because the timescale of $\boldsymbol{v}$ is much shorter than that of ψ, we may set $\partial \boldsymbol{v}/\partial t = 0$ in (2.3) as a very good approximation, and may express $\boldsymbol{v}$ as [58]

$$-\eta_0\, \nabla^2 \boldsymbol{v} = \left[-\psi\, \boldsymbol{\nabla} \frac{\delta}{\delta \psi} F + \boldsymbol{\zeta}_R \right]_\perp \tag{2.7}$$

where $[\cdots]_\perp$ denotes taking the transverse part (perpendicular to the wave vector $\boldsymbol{q}$ in the Fourier space). The same approximation is widely used also for colloidal systems (the Stokes approximation).

In renormalization group theory we decrease the upper cut-off wavenumber Λ of the fluctuations by averaging over the small-scale fluctuations, and examine how the coefficients in the dynamical model (as well as those in the free energy F) are changed or renormalized [10]. Systematic analysis is possible here if use is made of the expansion in $\epsilon = 4 - d$. In our model the following static and dynamical quantities tend to universal numbers:

$$g_0 = K_d u_0/\Lambda^\epsilon \to \frac{2}{3}\epsilon + \cdots \tag{2.8}$$

$$f_0 = K_d k_B T_c/L_0\eta_0\Lambda^\epsilon \to \frac{24}{19}\epsilon + \cdots \tag{2.9}$$

where the coefficients are functions of Λ, and $K_d = (2\pi)^{-d}2\pi^{d/2}/\Gamma(d/2)$. If the fluid is sufficiently close to the critical point, the above limits are attained even for $\Lambda \gg \xi^{-1}$, and the nonclassical critical behaviour follows. Then the renormalized coefficients are obtained at $\Lambda = \xi^{-1}$ because the fluctuation effects are weak for $\Lambda < \xi^{-1}$. In accord with this, the Ginzburg criterion, under which the mean-field theory holds, is given by $K_d u_0 \xi^\epsilon \ll 1$. It is known that in many polymer blends the above asymptotic limits can be attained only extremely close to the critical point, because u_0 is very small for $\Lambda \sim \xi_0^{-1}$ and/or η_0 is very large [13, 58]. On the other hand, the mode-coupling theory is a self-consistent decoupling scheme originally constructed in three dimensions [9]. In these theories, if the fluctuations with wavenumbers larger than the inverse correlation length ξ^{-1} are coarse grained, we obtain the usual hydrodynamic equations but with singular transport coefficients. For low-molecular-weight fluids, the predictions of these two theories turned out to be surprisingly close to each other, and agree excellently with experiments. One of the simplest results of the mode-coupling theory is that the diffusion constant at long wavelengths ($q\xi \ll 1$) is given by

$$D = k_B T_c/6\pi\eta\xi \tag{2.10}$$

which is consistent with (2.9) and is analogous to the Einstein–Stokes formula for the diffusion constant of a Brownian particle. The renormalized viscosity η has a nearly logarithmic singularity with a small amplitude, so it is not very different from the background value η_0 in (2.3). The characteristic lifetime of the fluctuations for $k \sim \xi^{-1}$ is thus

$$\tau_\xi = \xi^2/D = (6\pi\eta/k_B T)\xi^3 \tag{2.11}$$

which increases strongly near the critical point. It can even be of the order of 1 s in near-critical binary fluids. If the wavenumber q of the composition fluctuations is larger than ξ^{-1}, the decay rate is almost independent of ξ:

$$\Gamma(q) \cong (k_B T/6\pi\eta)q^3 \tag{2.12}$$

which has been confirmed by dynamical light scattering.

2.2. The strong-shear regime in one-phase states

In near-critical fluids, the main effect of shear is to deform the fluctuations by position-dependent convection. S is the hydrodynamic deformation rate, so we should compare the average decay rate of the fluctuations and S to find a weak-shear regime, $S\tau_\xi < 1$, and a strong-shear regime, $S\tau_\xi > 1$. Hereafter we are interested in the strong-shear regime, $S\tau_\xi > 1$, in which the critical fluctuations are drastically altered by shear before they dissipate thermally. It is convenient to introduce a characteristic wavenumber k_c via $\Gamma(k_c) = S$. Using (2.12) we obtain

$$k_c = (6\pi\eta/k_B T)^{1/3}S^{1/3}. \tag{2.13}$$

Then, by setting $k_c\xi = k_c\xi_0\tau_s^{-\nu}$, we may introduce a crossover reduced temperature τ_s as follows [19, 59]:

$$\tau_s = (6\pi\eta\xi_0^3/k_BT)^{1/3\nu}S^{1/3\nu} \propto S^{0.54}. \tag{2.14}$$

Slightly different definitions of k_c and τ_s follow if use is made of the dynamical renormalization group theory. The critical fluctuations are strongly deformed by shear in the long-wavelength region $q < k_c$.

Let us then calculate the steady-state structure factor for $r_0 > 0$. We start with the mean-field approximation or linearizing the dynamical equation (2.2). In the Fourier space it reads

$$\frac{\partial}{\partial t}\psi_{\boldsymbol{q}} = Sq_x\frac{\partial}{\partial q_y}\psi_{\boldsymbol{q}} - L_0q^2(r_0+q^2)\psi_{\boldsymbol{q}} + \theta_{R\boldsymbol{q}}. \tag{2.15}$$

The fluctuations are simultaneously convected by shear, and thermally dissipated with the decay rate (in the mean-field theory) given by

$$\Gamma(q) = L_0q^2(r_0+q^2). \tag{2.16}$$

The steady-state structure factor $I(\boldsymbol{q})$ satisfies

$$\left[2\Gamma(q) - Sq_x\frac{\partial}{\partial q_y}\right]I(\boldsymbol{q}) = 2L_0q^2. \tag{2.17}$$

The right-hand side arises from the thermal noise term $\theta_{R\boldsymbol{q}}(t)$, giving rise to the Ornstein–Zernike form $I_{OZ}(q) = 1/[r_0+q^2]$ without shear. The simplest way to examine the shear effect is to expand $I(\boldsymbol{q})$ in powers of S as follows:

$$I(\boldsymbol{q})/I_{OZ}(q) = 1 - 2q_xq_yI_{OZ}(q)S/\Gamma(q) + \cdots. \tag{2.18}$$

Thus the intensity increases most in the directions in which $q_x = -q_y$ in the q_x–q_y plane. Certainly, the shear effect becomes important when the (mean-field) strong-shear condition $S > L_0r_0^2$ holds. Generally, taking into account the convection due to shear, we may solve (2.17) in the following integral form:

$$I(\boldsymbol{q}) = \int_0^\infty \mathrm{d}t\ \exp\left[-2\int_0^t \mathrm{d}t_1\ \Gamma(|\boldsymbol{q}(t_1)|)\right]2L_0\boldsymbol{q}(t)^2 \tag{2.19}$$

in terms of a deformed wave vector defined by

$$\boldsymbol{q}(t) = \boldsymbol{q} + Stq_x\boldsymbol{e}_y \tag{2.20}$$

which is equal to $\tilde{\boldsymbol{q}}(-t)$ introduced below (1.6). Because (2.19) is complex, we give an approximate expression interpolating between various limiting cases of (2.19):

$$I(\boldsymbol{q}) \cong 1/[r_0 + ck_c^{8/5}|q_x|^{2/5} + q^2] \tag{2.21}$$

where $c \sim 1$, and k_c is determined by $L_0k_c^4 = S$ in the mean-field theory. Notice that $I(\boldsymbol{q}) \sim k_c^{-8/5}|q_x|^{-2/5}$ for most of the wave vectors smaller than k_c in strong shear (which means $r_0 < k_c^2$ in the mean-field theory). Light scattering experiments supported the above structure factor [17, 18]. A small-angle neutron scattering experiment was also performed on a low-molecular-weight polymer blend [60].

We thus find that $I(\boldsymbol{q})$ is suppressed below the equilibrium level, and the perturbation theory on the basis of (2.21) indicates that the critical dimensionality is lowered from 4 to 2.4 in strong shear. The precise meaning of this statement is that we may linearize the dynamical equations once we have eliminated the fluctuations with wavenumbers larger than k_c in three dimensions. That is, the lower cut-off wavenumber of the singular fluctuation

contributions is k_c in strong shear, while it is ξ^{-1} near equilibrium. For example, the renormalized kinetic coefficient in strong shear is

$$L = k_B T/6\pi\eta k_c \propto S^{-1/3}. \tag{2.22}$$

Obviously, if k_c is replaced by ξ^{-1}, the renormalized kinetic coefficient near equilibrium is obtained. The structure factor after the renormalization is roughly of the form

$$I(\boldsymbol{q}) \cong 1/[A(T - T_c(S)) + ck_c^{8/5}|q_x|^{2/5} + q^2] \tag{2.23}$$

with

$$A = \xi_0^{-2}\tau_s^{2\nu-1}/T_c \tag{2.24}$$

where k_c and τ_s are defined by (2.13) and (2.14). Again, if τ_s in equation (2.24) is replaced by $(T - T_c)/T_c$ and the limit $S \to 0$ is taken, we obtain the equilibrium result $A(T - T_c) \to \xi^{-2}$.

In near-critical fluids, the statical and dynamical renormalization effects are crucial, leading to (2.22) and (2.23). There are also systems in which the renormalization effects are negligible. As an extreme example, Dhont and Verduin [27] have examined shear effects in near-critical colloidal systems with attractive interaction superposed onto the hard-core repulsion, in which $\xi_0 = 2000$ Å and the mean-field theory holds.

2.3. The shift of the critical temperature

Next we discuss the critical temperature $T_c(S)$ in shear flow. We define the inverse susceptibility $r = 1/I(\boldsymbol{q})$ in the limit where $q_x = 0$ and $q \to 0$. It vanishes at $T = T_c(S)$, and differs from the coefficient r_0 in F given in (2.1). The difference $\Delta r = r - r_0$ arises first from the quartic term in F as follows:

$$(\Delta r)_s = \frac{1}{2}u_0 \int_{\boldsymbol{q}} \frac{1}{q^2} + \frac{1}{2}u_0 \int_{\boldsymbol{q}} \left(I(\boldsymbol{q}) - \frac{1}{q^2} \right) + \cdots \tag{2.25}$$

and secondly from the hydrodynamic interaction as follows:

$$(\Delta r)_h = \left(1 - \frac{1}{d}\right)(k_B T_c/\eta_0 L_0) \int_{\boldsymbol{q}} \frac{1}{q^2}(1 - q^2 I(\boldsymbol{q})) + \cdots \tag{2.26}$$

where $\int_{\boldsymbol{q}}(\cdots) = (2\pi)^{-d} \int \mathrm{d}\boldsymbol{q}\ (\cdots)$, and $I(\boldsymbol{q})$ is the structure factor at the critical point. We may derive (2.26) readily from the Kawasaki expression (2.7). Because shear flow suppresses the fluctuations, the second term of $(\Delta r)_s$ is negative and $(\Delta r)_h$ is positive, while they vanish in equilibrium.

In our original theory [15], we considered low-molecular-weight fluids, and calculated the shift of T_c assuming that the asymptotic limits (2.8) and (2.9) are attained for Λ much larger than k_c. Let us explain our result in this case using the ϵ-expansion. We note that the dominant contributions in the last two integrals of (2.25) and (2.26) arise from $q \sim k_c$, so by using (2.8) and (2.9) at a value of $\Lambda \sim k_c$ we obtain

$$(\Delta r)_s = \frac{1}{2}u_0 \int_{\boldsymbol{q}} \frac{1}{q^2} - 0.0442\,\epsilon k_c^2 \tag{2.27}$$

$$(\Delta r)_h = 0.1274\,\epsilon k_c^2. \tag{2.28}$$

Using (2.23) and (2.24) and summing these two contributions, we obtain

$$(T_c(S) - T_c(0))/T_c = (0.0442 - 0.1274)\epsilon\tau_s = -0.0832\,\epsilon\tau_s \tag{2.29a}$$

where τ_s is defined by (2.14). In three dimensions we expect

$$(T_c(S) - T_c(0))/T_c \sim -0.1\,\tau_s. \tag{2.29b}$$

The equilibrium critical temperature $T_c(0)$ is already shifted downwards from the mean-field critical temperature, which is simply the first term of (2.25) for small u_0. Shear suppresses the critical fluctuations and reduces this contribution, giving rise to the second term of (2.25). The nonlinear hydrodynamic interaction accelerates the diffusive decay of the fluctuations, leading to a larger downward shift of T_c.

Beysens *et al* detected a downward shift from the turbidity and the structure factor, with $\boldsymbol{q}$ perpendicular to the flow. It was proportional to $S^{0.53}$, but four times smaller than the result (2.29) at $\epsilon = 1$ in a few critical binary mixtures [18], so this aspect remains undecided. We note that it is difficult to determine the small shift definitively in usual binary mixtures, because the scattering is suppressed even at $T = T_c(S)$ as shown in (2.23), and does not grow indefinitely below $T_c(S)$ due to formation of stringlike domains, as will be explained in the next subsection.

Hashimoto *et al* [61–67] used a ternary mixture of polystyrene (PS) and polybutadiene (PB) in a common solvent of dioctylphthalate (DOP) to find a downward shift $(T_c(S) - T_c(0))/T_c \sim A_c\tau_s$ with $\tau_s \propto S^{0.5}$ and $A_c \cong 0.06$ [62]. That is, the scattering intensity above $T_c(S)$ perpendicular to the flow ($q_x = 0$) was expressed as

$$1/I(q) \cong \xi_0^{-2}(T - T_c(0))/T_c + A_c k_c^2 + q^2. \tag{2.30}$$

The second term gives rise to the downward shift. On the other hand, shear-induced homogenization took place at the same condition $T = T_c(S)$ if shear was increased from two-phase states at fixed T below $T_c(0)$. In their system the polymer volume fraction $\phi = \phi_{PS} + \phi_{PB}$ is of the order of the overlapping value, and the fluid may be treated as a binary mixture of weakly interacting PS-rich blobs and PB-rich blobs [67]. The space scale and timescale are much more enlarged than for usual binary mixtures, as $\tau_\xi \sim 1$ s even for $T - T_c \sim 10$ K and $\xi_0 \sim 50$ Å. The crossover reduced temperature τ_s in (2.14) is three or four orders of magnitude larger than for usual binary mixtures. In the temperature region investigated, the static properties are described by mean-field theory, whereas the diffusion constant $D_{mol} = L_0|r_0|$ of molecular origin and that, $D_{hyd} = k_B T/6\pi\eta\xi$, from the hydrodynamic interaction are not very different, as $D_{hyd}/D_{mol} \sim 0.2$–0.5 [62]. We believe that the observed downward shift should be due to the hydrodynamic interaction, which is consistent with (2.26). Very recently Yu *et al* [68] have used fluorescence and phase-contrast microscopy on a similar ternary mixture of PS + PB in DOP, and have reported that the shift tends to saturate at very high shear.

We note that the shift (2.29) is calculated on the rather special assumption of the asymptotic limits (2.8) and (2.9). However, they may not be satisfied in polymeric fluids, on which a number of shear flow experiments have been performed. We need to know the details of the critical fluctuations, the relevance of the hydrodynamic interaction, and the degree of viscoelasticity to reliably estimate the shift of the critical temperature. Polymer blends should exhibit complicated crossover effects in shear, depending on the distance to the critical point and the molecular weights, etc (where complexity is further increased in the presence of large asymmetry between the two components) [69–72].

Here, we also make a comment on the shear-induced shift of the transition temperature in the microphase separation in diblock copolymers. In such systems the structure factor has a maximum at an intermediate wavenumber q_m, and the nonlinear hydrodynamic interaction is not relevant [33]. Cates and Milner [34] calculated an upward shift from (2.25) using the bare u_0, neglecting the renormalization effect and the hydrodynamic interaction. Their prediction was in qualitative agreement with subsequent scattering experiments [35].

2.4. Spinodal decomposition in shear

More dramatic are the effects of shear in the unstable temperature and composition region. This problem is of technological importance in polymer systems. Beysens and Perrot performed a spinodal decomposition experiment on a near-critical binary mixture below T_c by periodically tilting a quartz pipe container [73]. Such a periodic shear was found to prevent the development of decomposition, resulting in a permanent spinodal ring of the scattered light. For steady shear, it was anticipated that domains are elongated in the flow direction as $S\tau\xi$ in an initial stage [74], which was in agreement with a subsequent light scattering experiment [19]. In figure 1 we show light scattering patterns obtained from a phase-separating fluid in shear, which are characterized by strong anisotropy (streak patterns) even in weak shear, $S\tau_\xi \ll 1$, below T_c [19, 59]. Computer simulations in two dimensions have also shown strong deformations of bicontinuous domain structures just after quenching [75–79]. Moreover, it has also been observed that spinodal decomposition is stopped in steady shear at a particular stage [61, 62], giving rise to dynamical stationary states. Such sates can be realized only by balance of the two competing mechanisms of thermodynamic instability and flow-induced deformation. In these two-phase states we may neglect the gravity effect when the domain size R is very small (as compared to the so-called capillary length). The Reynolds number Re of a domain is given by $Re = \rho SR^2/\eta$, and is very small near the critical point [16]. (Far from the critical point we may well encounter the opposite limit $Re \gg 1$, where the effect of inertia is crucial [16, 80].)

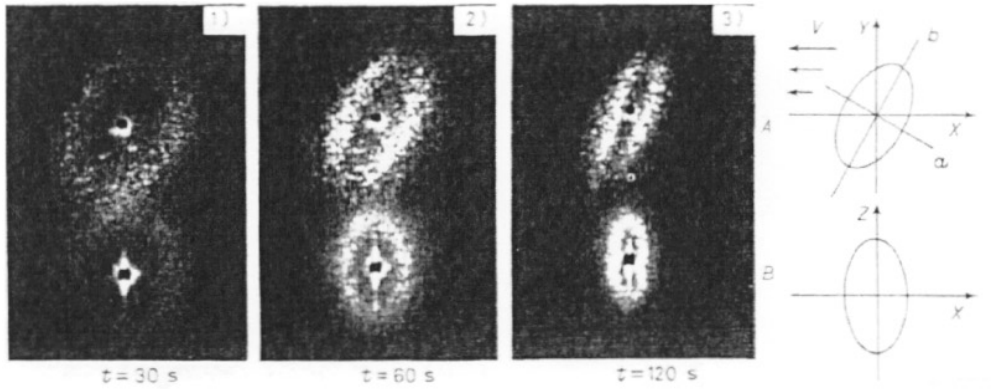

Figure 1. The time evolution of light scattering patterns from a phase-separating near-critical binary mixture at the critical composition [19]. Here $S = 0.035\ \mathrm{s}^{-1}$ and $T_c - T \sim 1$ mK, so $S\tau_\xi \sim 0.01$. The upper patterns (A) are those in the q_x–q_y plane, while the lower ones (B) are those in the q_x–q_z plane.

Unfortunately, detailed information cannot be gained from scattering alone, so some theoretical speculations were advanced regarding the domain morphology giving rise to streak patterns [81]. Recently Hashimoto *et al* [82] have taken microscope pictures of a DOP solution mentioned in subsection 2.3 to investigate the ultimate bicontinuous morphology in shear in real space as shown in figure 2. They have found that domains are elongated into extremely long cylinders in steady states except for in the case of extremely weak shear. For $S\tau_\xi < 1$, such stringlike domains still contain a number of random irregularities undergoing frequent break-up, interconnection, and branching, although the overall structure is kept stationary. For $S\tau_\xi > 1$ the continuity of the strings increases, and extends even macroscopically in the flow direction. The scattering intensity perpendicular to the flow is

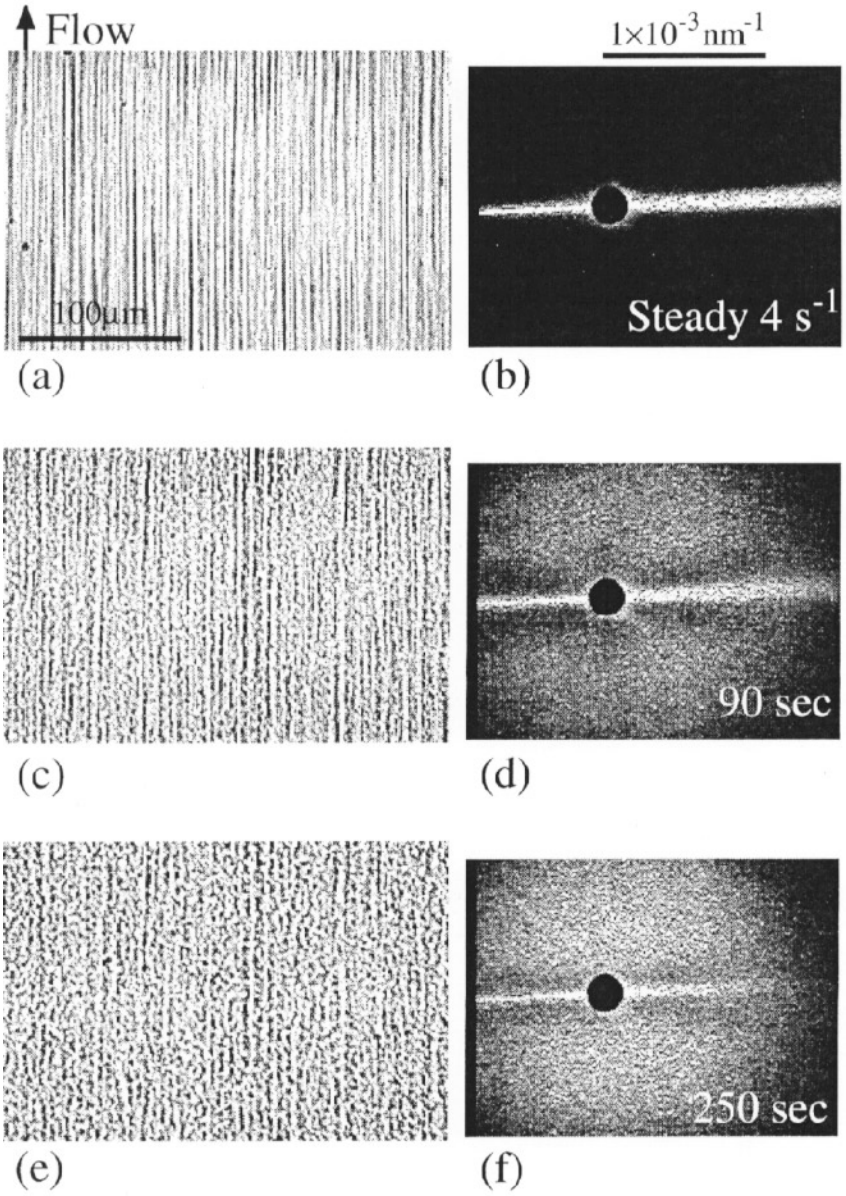

Figure 2. Microscope images ((a), (c), (e)) and corresponding light scattering patterns ((b), (d), (f)) for a PS/PB(80:20)/DOP 3.3 wt% solution at $T_c - T = 10$ K (taken by Hashimoto's group). Here (a) and (b) were obtained under steady shear at 4 s^{-1}, while (c) to (f) were obtained at 90 s and 250 s after cessation of the shear. We can see break-up of cylindrical domains into droplets, which occurs on the timescale of $\eta\xi_\perp/\sigma$, where σ is the surface tension and $\xi_\perp$ is the cylinder diameter.

proportional to the squared Lorentzian form $1/[1 + (q\xi_\perp)^2]^2$ due to cylindrical domains, where $\xi_\perp$ represents the diameter of the cylinders, and decreases with shear as

$$\xi_\perp \cong [10/q_m(0)](S\tau_\xi)^{-\alpha} \tag{2.31}$$

where $q_m(0)$ is the peak wavenumber in spinodal decomposition without shear, and $\alpha = 1/4 - 1/3$. For very large shear $S \gtrsim 10^2/\tau_\xi$, the diameter ultimately becomes of the order of the interface thickness, and the contrast between the two phases vanishes, resulting in shear-induced homogenization (at $T = T_c(S)$ for the case at the critical composition).

Very recently, Hobbie *et al* [83] studied the dynamics of the formation of the string phase in a DOP solution after application of shear. Also, for usual binary mixtures, Hamano has observed extreme elongation of domains in strong shear $S\tau_\xi \gtrsim 1$ [84]. Note that the streak scattering patterns in DOP solutions closely resemble those in usual binary mixtures [19, 59]. We should also mention that microscope pictures of stringlike domains were reported for polymer blends [85].

We note that the surface tension is extremely small ($\lesssim 10^{-4}$ cgs) in Hashimoto's case and those of usual binary mixtures. We believe that shear can suppress surface undulations of cylindrical domains for very low surface tension. Such undulations grow, resulting in break-up of cylinders into droplets in the absence of shear (the Tomotika instability [86]). Figure 2 shows a dramatic example observed after cessation of the shear. Interestingly, this capillary-driven instability is in essence the coarsening mechanism of late-stage spinodal decomposition at the critical composition [87]. Rheologically, there should be no appreciable increase $\Delta\eta$ of the macroscopic viscosity in the string phase, where the surfaces do not resist the flow. This point will be discussed again in subsection 2.6.

Very recently, spinodal decomposition under shear flow has been studied by molecular dynamics (MD) simulation of a two-dimensional Lennard-Jones system consisting of 40 000 particles [79]. This has involved applying a very large shear realizable only in MD simulations, and examination of elongated domain morphologies below T_c. We notice that the simulation [79] has been performed in a regime with a relatively large Reynolds number, $Re = \rho S R^2/\eta \gtrsim 1$, with significant velocity field fluctuations.

We may also consider spinodal decomposition under oscillating shear, $S(t) = S_0 \cos(\omega t)$. Krall *et al* [88] pointed out a new bifurcation effect under periodic shear on the basis of a phenomenological domain growth theory of Doi and Ohta [89]. That is, if the maximum shear strain $f = S_0/\omega$ is larger than a critical value f_c, the shear distortion is effective enough, and the domain growth can be stopped, resulting in a periodic two-phase state. If $f < f_c$, the shear cannot stop the growth leading to macroscopic phase separation. Interestingly, a similar bifurcation was found in a spinodal decomposition experiment under periodic quenching [90].

2.5. Nucleation in shear

2.5.1. Droplet break-up and coagulation in shear. We then slightly lower the temperature T below the coexistence temperature T_{cx} by $\delta T = T_{cx} - T$ in the off-critical case. To observe appreciable droplets of the new phase, the critical droplet must not be torn by shear, and hence we require

$$R_c < R^* \tag{2.32}$$

where $R_c \sim \xi/\Delta$ is the critical radius of nucleation and

$$R^* \sim \sigma/\eta S \tag{2.33}$$

is the Taylor break-up size [91–93]. Δ ($=\Delta(0)$) is the initial supersaturation, much smaller than 1, and is related to δT and $\Delta T = T_c - T_{cx}$ by $\Delta \cong \frac{1}{6}(\delta T/\Delta T)$ near criticality. Then, a necessary condition for observing noticeable droplets follows [16, 81, 94]:

$$S\tau_\xi < \Delta \ll 1. \tag{2.34}$$

This gives an upper limit for the shear, $S^* \sim \Delta/\tau$, at each δT, or a lower limit for the quench depth

$$\delta T^* \sim S\tau(\Delta T) \propto S(\Delta T)^{1-3\nu} \tag{2.35}$$

at each S, in order to have droplets. This simple criterion has been confirmed for binary mixtures under gentle stirring [95, 96] and uniform shear [97].

The key quantity in the initial stage of nucleation is the nucleation rate [11, 12]

$$J \propto \exp(-a(\Delta T/\delta T)^2) \tag{2.36}$$

where a is a number of order 1. It is the probability of finding droplets with radius larger than R_c per unit volume and per unit time. It is known that J can be of order 1 when δT is equal to the classical Becker–Döring limit

$$\delta T_{BD} \cong 0.15\,\Delta T. \tag{2.37}$$

We note that $\delta T^* < \delta T_{BD}$ for very weak shear, which satisfies (2.34). If this inequality holds, droplets will emerge at $\delta T = \delta T_{BD}$ on increasing δT from zero, but droplets will disappear at $\delta T = \delta T^*$ on decreasing δT from a state in which droplets pre-exist. This hysteretic behaviour was observed by Min and Goldburg [97], as shown in figure 3. Namely, the point where $F \cong 1$ on the branch H corresponds to the appearance of droplets, while the point where $F \cong 1$ on the branch C corresponds to the disappearance of droplets.

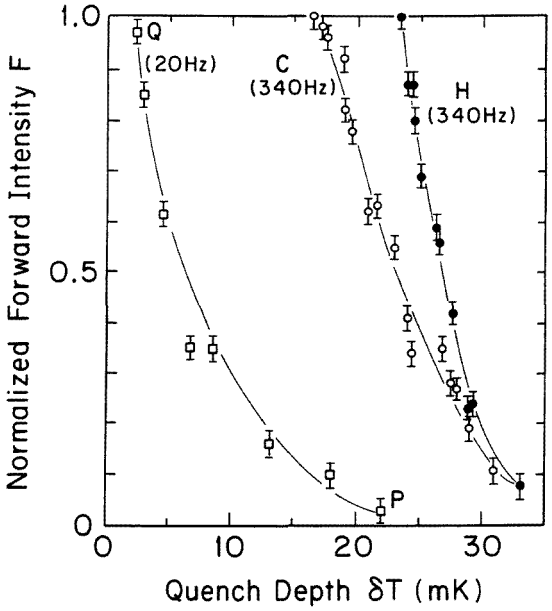

Figure 3. The normalized forward intensity F (the transmittency of light) from an off-critical binary mixture as a function of the quench depth δT [97]. The curves H, C, and PQ correspond to $S = 340, 340,$ and 20 s^{-1}. The lines are a guide to the eye. On the branch PQ the experiment was started at the point P in an opaque state, and was ended at the point Q where droplets disappeared due to the break-up mechanism. The branch H was started at the point where $F \cong 1$, where the nucleation rate is appreciable. The branch C was ended at the point where $F \cong 1$, due to the break-up mechanism.

Another important mechanism is the flow-induced coagulation of droplets [98, 99]. It is known that in flow, both laminar and turbulent, a droplet collides with others on a timescale

of order $1/\phi S$ (the mean free time) where ϕ is the droplet volume fraction. This estimation is valid when the sizes of the colliding droplets are of the same order. On the other hand, flow-induced collisions rarely occur between droplets with very different sizes, because the smaller one moves on the stream line of the velocity field around the larger one without appreciable diffusive motion for $Pe \gg 1$ [100, 101]. Due to this coagulation, the average droplet size grows as [99, 102]

$$\left(\frac{\partial R}{\partial t}\right)_{coll} \sim S\phi R \tag{2.38}$$

leading to an exponential growth of R.

For aggregating colloidal systems, the above exponential growth is well known [102]. Simulations of colloid aggregates have shown deformation, rupture, and coagulation of clusters in shear flow [103, 104]. These hydrodynamic effects are of great technological importance for two-phase polymers [105], in particular in the presence of copolymers [106].

Here we raise a fundamental question as to the existence of metastability itself in relatively large shear for which (2.34) is not satisfied. That is, if δT is increased in such shear, droplet formation will be suppressed, because localized droplets larger than R^* cannot be stable. In particular, if $S\tau_\xi \sim 1$, R_c becomes of order ξ and the suppression is complete, in the sense that phase separation can be triggered only by instability of plane-wave fluctuations. That is, a spinodal point becomes well defined in such relatively large shear as the unique onset point of phase separation. Recall that the spinodal point obtained in the mean-field theory has no definite theoretical meaning for quiescent fluids [11, 12].

2.5.2. Droplet size distribution in shear. Under (2.34), a nearly stationary distribution of droplets is realized after a long relaxation time [97]. Remarkably, the size distribution is peaked at $R \cong R^*$ and, once such a distribution is established, further time development of the droplet distribution becomes extremely slow. Min and Goldburg [97] have found that the supersaturation Δ tends to a finite value $\Delta(S)$ dependent on S by gradually increasing δT from zero, which corresponds to the branch H in figure 3. It can be determined because the droplet volume fraction is $\phi = \Delta(0) - \Delta(S)$. Though such a state is nearly stationary, there is still a diffusive current onto each droplet from the surrounding metastable region. Each droplet will grow above R_c and break into smaller droplets, which will then start to grow again or dissolve into the metastable region depending on whether their radii are larger or smaller than R_c. Each droplet will also collide with another one on the timescale of $1/S\phi$. The evolution of the droplet size distribution is therefore very complex, and the observed quasi-stationarity is produced by a delicate balance among these processes. Alternatively, we may also start with an opaque state in which δT is sufficiently large and $\Delta(S) \cong 0$ (or $\phi \cong \Delta(0)$). Then, by gradually decreasing δT at fixed S, a nearly stationary state will be obtained, which corresponds to the branch C in figure 3. Interestingly, it has been found to be more opaque and to have a larger droplet volume fraction (or a smaller supersaturation) than in the reverse case of increasing δT from zero.

Hashimoto *et al* [65, 66] have observed similar hysteresis in off-critical DOP solutions by increasing or decreasing S over a very wide range with δT fixed. First, they increased S from an opaque state with droplets to reach a transparent state without droplets at $T_{spi}(0) - T \propto S$, where $T_{spi}(0)$ is the cloud-point temperature at zero shear. We believe that this disappearance of droplets should have been caused by the Taylor break-up mechanism, though the difference between $T_{spi}(0)$ and the temperature T_{cx} on the coexistence curve is not clarified in their work. Second, they decreased S from a disordered state homogenized by large shear to reach a spinodal-like point at which $T_{spi}(0) - T \propto S^{1/2}$, and below which

droplets appear. However, they found that the quasi-steady states reached in the decreasing branch are still slowly evolving towards the steady states reached in the increasing branch on timescales of several hours. We believe that the experiments performed by Hashimoto *et al* and those performed by Goldburg and Min are consistent with each other.

2.5.3. Acceleration of droplet growth in shear. To analyse their experiment, Baumberger *et al* [107] argued that the growth of an isolated droplet in a metastable fluid can be considerably accelerated even in very weak shear by an advection mechanism. If the growth is slow, the composition ψ outside the droplet is determined by a quasi-static condition:

$$\boldsymbol{u} \cdot \boldsymbol{\nabla} \psi + D \nabla^2 \psi = 0 \tag{2.39}$$

where $\boldsymbol{u}$ is the average flow tending to a simple shear flow far from the droplet. The relative importance of the two terms in (2.39) is given by the Peclet number

$$Pe = SR^2/D = S\tau_\xi (R/\xi)^2. \tag{2.40}$$

We have $Pe > S\tau_\xi/\Delta^2$ for $R > R_c$, and $Pe \sim 1/St_\xi$ at the break-up size $R \sim R^*$. Thus $Pe \gg 1$ can hold over a sizable time interval even under (2.32) or (2.34). The deviation from the spherical shape is small for $R \ll \sigma/\eta S$ or for $R \ll R^*$. For $Pe \gg 1$ it is important that the composition gradient is localized in a thin layer, with a thickness ℓ_S given by

$$\ell_S \sim (D/S)^{1/2} \sim R/\sqrt{Pe} \tag{2.41}$$

around the droplet. This relation follows from the balance between the two terms in (2.39). As a result, the diffusion current onto the droplet from the metastable fluid is enlarged by $\ell_S/R \sim Pe^{1/2}$ as compared to the case where $Pe \ll 1$ [108, 109], so the usual Lifshitz–Slyozov equation [110] is modified as follows:

$$\frac{\partial}{\partial t} R \sim \frac{D}{R}\left(\Delta - \frac{2\alpha}{R}\right) Pe^{1/2} \sim (SD)^{1/2}\left(\Delta - \frac{2\alpha}{R}\right) \tag{2.42}$$

where α is a capillary length ($\sim\xi$). Thus the timescale of the initial stage can be considerably accelerated by the convection effect. However, the critical radius $R_c = 2\alpha/\Delta$ is unchanged by very weak shear, and there seems to be no drastic change in the nucleation rate, although this is not confirmed.

The above mechanism is important in systems with a small diffusion constant such as polymer blends. As another similar effect we note that, if surfactant molecules are added to an oil–water two-phase system, they can be advected onto the oil–water interfaces efficiently in shear flow, leading to shear-induced emulsification. Systematic experiments in these cases should be interesting.

2.6. Rheology in strong shear and in two-phase states

The fluctuations of the order parameter ψ give rise to the following additional shear stress [114, 113]:

$$S\,\Delta\eta = -k_B T \langle (\partial\psi/\partial x)(\partial\psi/\partial y)\rangle \tag{2.43}$$

where the average is taken in a system under shear. Other important quantities include the normal-stress differences:

$$N_1 = \sigma_{xx} - \sigma_{yy} = k_B T \langle (\partial\psi/\partial x)^2 - (\partial\psi/\partial y)^2\rangle \tag{2.44}$$

$$N_2 = \sigma_{yy} - \sigma_{zz} = k_B T \langle (\partial\psi/\partial y)^2 - (\partial\psi/\partial z)^2\rangle. \tag{2.45}$$

In the one-phase region, the above quantities may be expressed as integrals in the wave-vector space using the structure factor $I(\boldsymbol{q})$. We find that $\Delta\eta$ is nearly logarithmic, varying as $\log(\xi/\xi_0)$ in weak shear and as $\log(1/k_c\xi_0)$ in strong shear. This crossover was first predicted by Oxtoby [111]. If use is made of the ϵ-expansion in strong shear, we obtain [112]

$$\eta = \eta_0 + \Delta\eta \propto (k_c\xi_0)^{-x_\eta} \propto S^{-x_\eta/d} \tag{2.46}$$

where $x_\eta = \epsilon/19 + \cdots$ is a small dynamical exponent. This shear rate dependence was measured by Hamano *et al* [115]. In weak shear, the normal-stress differences are proportional to S^2 and are very small. In strong shear, the wave-vector integrals in (2.43)–(2.45) are of order ηk_c^d, and

$$N_1 = 0.046\epsilon\eta S \qquad N_2 = -0.032\epsilon\eta S \tag{2.47}$$

to first order in ϵ. (Note that N_1 and N_2 are even functions of S, while the shear stress σ_{xy} is odd. If we allow the case where $S < 0$, we should use $|S|$ in (2.46) and (2.47).)

When a near-critical fluid is undergoing phase separation, larger stress contributions arise from interface deformations [113] because $(\boldsymbol{\nabla}\phi)(\boldsymbol{\nabla}\phi)$ behaves like a δ-function near the interface multiplied by the tensor $\boldsymbol{nn}$, where $\boldsymbol{n} = (n_x, n_y, n_z)$ is the normal unit vector. In particular, in weak shear, interfaces are sharp and (2.43) yields a well-known expression [116, 113, 117]:

$$(\Delta\eta)_{int} = -\frac{1}{S}\sigma \int \mathrm{d}a\ n_x n_y \tag{2.48}$$

where σ is the surface tension, da is the surface element, and the surface integral is within a unit volume. This surface contribution is the sole change of the macroscopic viscosity in Newtonian two-phase fluids with the same viscosity. The problem is much more complicated if the two phases have different viscosities [116, 118]. Similarly,

$$(N_1)_{int} = \sigma \int \mathrm{d}a\ (n_x^2 - n_y^2) \qquad (N_2)_{int} = \sigma \int \mathrm{d}a\ (n_y^2 - n_z^2). \tag{2.49}$$

If we suppose an assembly of largely deformed droplets near the break-up condition $R \sim R^*$, as given in (2.33), we estimate $\langle -n_x n_y\rangle \sim \langle n_x^2 - n_y^2\rangle \sim 1$, and

$$(\Delta\eta)_{int} \sim \phi\sigma/SR \sim \phi\eta \tag{2.50}$$

$$(N_1)_{int} \sim (N_2)_{int} \sim \eta S\phi \tag{2.51}$$

where the surface areal density is of order ϕ/R in terms of the volume fraction ϕ of the droplet phase. Because (2.50) is independent of shear, it is analogous to well-known expressions for the macroscopic viscosity of suspensions or emulsions in the zero-shear limit [116]. However, in our case, droplets are substantially deformed, so the rheology is strongly nonlinear. The behaviour of N_1 and N_2 is marked, because they are nearly zero for one-phase states, and jump to large values after quenching. Doi and Ohta re-derived the above results by setting up constitutive equations for the interfacial stress tensor [89].

Krall *et al* [88] measured $\Delta\eta(t)$ for a near-critical binary mixture using a viscometer in which shear was oscillated and damped in time. After a pressure quench at $t = 0$, $\Delta\eta(t)$ increased on the timescale of τ_ξ in accord with (2.50). It tended to a constant for the droplet case, whereas it slowly decayed to zero in the critical (bicontinuous) case after a long time ($\sim$20 s). The origin of this slow decay was ascribed to the fact that shear cannot stop coarsening after a certain decrease of the oscillating amplitude in their viscometer (see the last comment in subsection 2.4). Subsequently, however, Hamano *et al* [119] observed the same decay of $\Delta\eta(t)$ in steady shear in a rotational viscometer. Because a sharp streak

scattering pattern emerges with $\Delta\eta(t) \to 0$, we may conclude that a string phase discussed in subsection 2 was realized in their critical quench cases. For such highly elongated domains, the interfaces are mostly parallel to the flow, and $n_x \cong 0$ in (2.48), leading to $\Delta\eta \cong 0$.

Recently, the rheology of phase-separating polymer blends has also been studied [120–122] particularly when the two phases are Newtonian and have almost the same viscosity. The observed $\Delta\eta$ and N_1 were in excellent agreement with the scaling relations (2.50) and (2.51). It is of great importance in polymer physics to understand the rheology in more complex two-phase states, such as in the case in which the viscosity difference between the two phases is large [118, 123], or the case in which viscoelasticity is crucial. The latter case will be discussed in subsection 3.5.

In aqueous surfactant solutions, marked increases of the viscosity and N_1 were observed, which was interpreted as arising from shear-induced aggregate formation or gelation [42]. In aqueous solutions of agarose, huge viscosity enhancement was also observed, in which gelation was probably induced upon phase separation [124]. In colloids near the critical point [125] and dense microemulsions near the percolation threshold [126], the viscosity has been reported to grow strongly, in contrast to the weak-viscosity singularity in the usual near-critical fluids. In such systems, near a phase transition, interesting nonlinear rheology might well be expected at high shear and/or in two-phase cases.

Simulations of simple fluids in two dimensions have also shown an increase of the viscosity in spinodal decomposition [75–77, 79]. In the MD study of a Lennard-Jones fluid [79], dynamical steady states with irregularly elongated domains have been attained. Simulations of fluids with internal structures in this direction should be of great importance. (An example for the viscoelastic case will be given at the end of section 3.)

2.7. Effects of stirring

Fluids can be mixed even by gentle stirring, so it is always used in experiments and in everyday life. Voronel and co-workers [127] measured the specific heat C_v under stirring in one-component fluids near the gas–liquid critical point. Surprisingly, they could observe a sharp peak of C_v even very close to the critical point, which would have been masked by the gravity effect in a quiescent fluid. To support their finding, we may argue [128] that the density stratification in gravity is much reduced from $-\rho g(\partial\rho/\partial p)_T$ to $-\rho g(\partial\rho/\partial p)_s$ under stirring. The ratio of these two quantities is $(\partial\rho/\partial p)_T/(\partial\rho/\partial p)_s = C_p/C_v$, and is very large near the gas–liquid critical point. This means that the entropy per unit mass s tends to be homogenized in stirred fluids despite the presence of a pressure gradient. There should also arise a vertical temperature gradient

$$\mathrm{d}T/\mathrm{d}z = -\rho g(\partial T/\partial p)_s \tag{2.52}$$

which is -0.9 mK cm^{-1} on earth in xenon. Also, in binary mixtures, if use is made of the derivative $(\partial T/\partial p)_{sX}$ at fixed composition X, we can predict the same temperature gradient. Cannell [129] first reported the presence of a temperature nonuniformity in stirred fluids in gravity. But there has been no systematic experiment to confirm the above predictions.

We may also examine critical phenomena and phase separation of near-critical binary mixtures in vigorous stirring or turbulence [130–133]. It is known that the maximum shear rate S_d in turbulence is given by $(\eta/\rho)k_d^2$, where

$$k_d = L_0^{-1} Re^{3/4} \tag{2.53}$$

is the Kolmogorov lower cut-off wavenumber, L_0 being the size of the largest eddies and Re being the Reynolds number, much larger than 1. We note that in the case of near-critical

fluids, the composition fluctuations have sizes much shorter than the size of the smallest eddies ($\sim 1/k_d$), and are most effectively strained by the smallest eddies. These eddies turn over on the timescale of $1/S_d$, during which the composition fluctuations are affected by the eddies. Experiments showed that there is no sharp phase transition in turbulence, and that the scattered light intensity increases gradually but dramatically as T is lowered below T_c. As in the case of laminar shear, there is a strong-shear regime determined by $\tau_\xi S_d > 1$, in which the fluctuations are strongly suppressed by random shear. If a fluid is further quenched below T_c into the weak-shear region $\tau_\xi S_d \ll 1$, the characteristic domain size should be given by

$$R \sim \sigma/\eta S_d \sim (\rho\sigma/\eta^2)k_d^{-2} \tag{2.54}$$

as for laminar shear [16]. Note that the above scenario holds only for $R < 1/k_d$, which is equivalent to the condition $\sigma < (\eta^2/\rho)k_d$. In fluids far from the critical point, this condition is not satisfied, where the Kolmogorov scaling yields [134, 99, 16]

$$R \sim (\rho\sigma/\eta^2)^{3/5}k_d^{-8/5} > k_d^{-1}. \tag{2.55}$$

Here, instead of the shear stress ηS_d, the typical pressure variation ($\sim\rho u_R^2$) over the distance R is balanced with the capillary force density ($\sim\sigma/R$), where u_R ($\propto R^{1/3}$) is the typical velocity of eddies with size R. An attempt has also been made to simulate phase separation using a time-dependent Ginzburg–Landau model in the presence of a model random velocity field [135].

We finally mention experiments by an Uzbekistan group [136]. They detected a peak in the specific heat deeply inside the coexistence curve in stirred off-critical fluids, where the peak height increased with increase in the degree of stirring. They claimed that a spinodal point can be reached in the presence of stirring, but it should be checked by more experiments. Their effect might be related to the question raised at the end of section 2.5.1.

3. Shear-induced phase separation

The effects of shear on polymeric systems are generally very complex [8]. As well as shear-induced mixing, application of shear or extensional flow sometimes induces a large increase of the turbidity, indicating shear-induced composition heterogeneities or demixing [137]. In polymer blends, these two tendencies can occur in the same polymer mixture, depending on the composition and temperature [70, 72]. Semidilute polymer solutions near the coexistence curve most unambiguously exhibit shear-induced demixing, as reviewed by Rangel-Nafaile *et al* in 1984 [138]. In particular, Krämer and Wolf [139] showed that the tendency towards demixing is dramatically intensified by increase of the molecular weight M ($\gtrsim 2 \times 10^6$) and the polymer volume fraction above the overlapping value. In such situations for non-Newtonian shear, significant shear-thinning behaviour has been observed in steady states. At very high shear, furthermore, an onset of shear-thickening behaviour was detected [140]. As will be discussed in the last part of this section, large stress fluctuations were also reported upon demixing by shear [5, 6, 141], suggesting the formation of gel-like aggregates under shear.

Recently, a number of scattering experiments have been performed on high-molecular-weight polymer solutions under shear (polystyrene (PS) + dioctylphthalate (DOP) solutions) [142–148], together with a dichroism experiment [57]. Theoretical efforts to understand this complex problem have also been made intensively [149–156]. We will review the recent theoretical progress together with some new analytic and numerical results. We mention three main theoretical ingredients that are being established. They are (i) a

dynamical coupling mechanism first applied to sheared polymer solutions by Helfand and Fredrickson [149, 153], (ii) a viscoelastic Ginzburg–Landau scheme [150, 151, 154, 155] with a conformation tensor as a new independent dynamical variable, and (iii) computer simulations [156] which would give insights into strongly fluctuating polymer solutions under shear. However, a number of puzzles remain unexplored in spinodal decomposition and nucleation with (and even without) shear below the coexistence curve.

We should also mention intriguing small-angle neutron scattering experiments on gels which are swollen and uniaxially expanded [157]. Heterogeneities of the crosslink structure are believed to induce frozen composition variations giving rise to abnormal butterfly scattering patterns [157–160], which are very similar to those from sheared polymer solutions in the q_x–q_z plane [143, 147, 159]. For both polymer solutions and gels, the problems encountered are those of the stress balance attained by composition changes in heterogeneous systems. The difference is that the crosslink structure is permanent in gels and transient in polymer solutions, which makes the problem simpler (though still complex) for gels [159].

3.1. Dynamical coupling between stress and diffusion

Semidilute polymer solutions become highly viscoelastic when the molecular weight is very large and when the polymer volume fraction ϕ exceeds the critical volume fraction $\phi_c = N^{-1/2}$, where N is the polymerization index (the number of segments on a chain), much larger than 1. We assume that the polymer volume fraction ϕ is much smaller than 1, and will replace the factor $1-\phi$ by 1 in many relations to follow. The viscosity η and the stress relaxation time τ dramatically increase with increasing ϕ and N, because a large network stress is produced due to entanglement even against small deformations. It has recently been recognized that the stress can influence spatial inhomogeneities of the composition through a dynamical coupling between stress and diffusion. This coupling gives rise to nonexponential relaxation of the time correlation function of the composition fluctuations near equilibrium [161–165].

To illustrate this new concept, let us consider a simple two-fluid model of polymer solutions [149–156, 166, 167]. The mass densities, ρ_p and ρ_s, of the polymer and the solvent are convected by their velocities, $\boldsymbol{v}_p$ and $\boldsymbol{v}_s$, as follows:

$$\frac{\partial}{\partial t}\rho_p = -\boldsymbol{\nabla}\cdot(\rho_p \boldsymbol{v}_p) \qquad \frac{\partial}{\partial t}\rho_s = -\boldsymbol{\nabla}\cdot(\rho_s \boldsymbol{v}_s). \tag{3.1}$$

The total density $\rho = \rho_p + \rho_s$ obeys the usual continuity equation with the momentum current $\rho\boldsymbol{v}$, where the average velocity $\boldsymbol{v}$ is defined by

$$\boldsymbol{v} = \rho^{-1}(\rho_p \boldsymbol{v}_p + \rho_s \boldsymbol{v}_s). \tag{3.2}$$

Most polymer solutions have a very small compressibility or are nearly incompressible. Therefore the density deviation $\delta\rho = \rho - \bar{\rho}$ from the average $\bar{\rho}$ is very small, and the continuity equation may be linearized as

$$\frac{\partial}{\partial t}\delta\rho = -\bar{\rho}\boldsymbol{\nabla}\cdot\boldsymbol{v}. \tag{3.3}$$

For simplicity, we further assume that the mass densities of pure polymer and solvent are the same. Then the mass fraction ρ_1/ρ coincides with ϕ. It obeys

$$\left(\frac{\partial}{\partial t} + \boldsymbol{v}\cdot\boldsymbol{\nabla}\right)\phi = -\boldsymbol{\nabla}\cdot(\phi(1-\phi)\boldsymbol{w}) \cong -\boldsymbol{\nabla}\cdot(\phi\boldsymbol{w}) \tag{3.4}$$

where

$$\boldsymbol{w} = \boldsymbol{v}_p - \boldsymbol{v}_s \tag{3.5}$$

is the relative velocity of the polymer and the solvent. The diffusion current is given by $\phi\boldsymbol{w}$. The two velocities $\boldsymbol{v}_p$ and $\boldsymbol{v}_s$ are expressed as

$$\boldsymbol{v}_p = \boldsymbol{v} + (1-\phi)\boldsymbol{w} \qquad \boldsymbol{v}_s = \boldsymbol{v} - \phi\boldsymbol{w} \tag{3.6}$$

so we have $\boldsymbol{v}_p \cong \boldsymbol{v} + \boldsymbol{w}$ and $\boldsymbol{v}_s \cong \boldsymbol{v}$ for $\phi \ll 1$.

The equations of motion for the two components are

$$\rho_p \frac{\partial}{\partial t}\boldsymbol{v}_p = -\rho_p \boldsymbol{\nabla}\mu_p - \zeta \boldsymbol{w} + \boldsymbol{F}_p \tag{3.7}$$

$$\rho_s \frac{\partial}{\partial t}\boldsymbol{v}_s = -\rho_s \boldsymbol{\nabla}\mu_s + \zeta \boldsymbol{w} + \eta_0 \nabla^2 \boldsymbol{v}_s. \tag{3.8}$$

Here we consider only very slow motion, and neglect temperature inhomogeneities. μ_p and μ_s are appropriately defined chemical potentials, and ζ is the coefficient of friction between the two components. $\boldsymbol{F}_p$ is the force arising from the network stress, so $\boldsymbol{F}_p \cong \boldsymbol{\nabla}\cdot \overleftrightarrow{\boldsymbol{\sigma}}_p$ in terms of the network stress tensor $\overleftrightarrow{\boldsymbol{\sigma}}_p$. η_0 is the solvent viscosity, much smaller than the solution viscosity η. The scaling theory [13] shows that ζ is of the following order:

$$\zeta \sim 6\pi\eta_0 \xi^{-2} \sim 6\pi\eta_0 b^{-2}\phi^2 \tag{3.9}$$

where $\xi \sim b/\phi$ is the thermal correlation length and b is the monomer size. From (3.7) and (3.8), the relative velocity $\boldsymbol{w}$ is governed by

$$\frac{\partial}{\partial t}\boldsymbol{w} = -\boldsymbol{\nabla}(\mu_p - \mu_s) - \zeta\left(\frac{1}{\rho_p} + \frac{1}{\rho_s}\right)\boldsymbol{w} + \frac{1}{\rho_p}\boldsymbol{F}_p. \tag{3.10}$$

The viscosity term ($\propto\eta_0$) in (3.8) has been neglected. In our problems, the characteristic frequencies are much lower than $\zeta(1/\rho_p + 1/\rho_s)$, so we may set $\partial\boldsymbol{w}/\partial t = \boldsymbol{0}$ in (3.10) to obtain

$$\boldsymbol{w} = (\rho_p\rho_s/\zeta\rho)\left[-\boldsymbol{\nabla}(\mu_p - \mu_s) + \frac{1}{\rho_p}\boldsymbol{F}_p\right]. \tag{3.11}$$

We substitute (3.11) into (3.4) by setting $\boldsymbol{F}_p = \boldsymbol{\nabla}\cdot\overleftrightarrow{\boldsymbol{\sigma}}_p$ and

$$\mu_p - \mu_s = \rho^{-1}\frac{\delta}{\delta\phi}F \tag{3.12}$$

where F is the free-energy functional, dependent on ϕ. The above relation will be justified by means of (3.62) and (3.63) below. Then we obtain

$$\left(\frac{\partial}{\partial t} + \boldsymbol{v}\cdot\boldsymbol{\nabla}\right)\phi = \boldsymbol{\nabla}\cdot L\left[\boldsymbol{\nabla}\frac{\delta F}{\delta\phi} - \frac{1}{\phi}\boldsymbol{\nabla}\cdot\overleftrightarrow{\boldsymbol{\sigma}}_p\right] \tag{3.13}$$

where

$$L = \phi^2/\zeta \sim b^2/6\pi\eta_0 \tag{3.14}$$

is the kinetic coefficient, which is independent of ϕ in the semidilute case. This equation implies that imbalance of the network stress ($\boldsymbol{\nabla}\cdot\overleftrightarrow{\boldsymbol{\sigma}} \neq \boldsymbol{0}$) leads to relative motion of the polymer and solvent. This form of the equation was originally derived for gels to analyse dynamical light scattering [167]. Helfand and Fredrickson [149] used the above form for sheared polymer solutions. Wittmann and Fredrickson [168] presented a formal theory using the projection operator method, and claimed that the dynamical coupling arises even on the

basis of the Rouse dynamics without entanglement. Similar efforts have also been made by Sun *et al* [169].

The average velocity is governed by

$$\bar{\rho}\,\frac{\partial}{\partial t}\boldsymbol{v} = -(\rho_p\,\boldsymbol{\nabla}\mu_p + \rho_s\,\boldsymbol{\nabla}\mu_s) + \boldsymbol{F}_p + \eta_0\,\nabla^2\boldsymbol{v} \tag{3.15}$$

where ρ is replaced by the average $\bar{\rho}$, and $\boldsymbol{v}_s$ in the last term is replaced by $\boldsymbol{v}$ because $\boldsymbol{v}_s \cong \boldsymbol{v}$ from (3.6). As in (2.7), we may further set in most cases

$$\partial\boldsymbol{v}/\partial t = 0 \qquad \boldsymbol{\nabla}\cdot\boldsymbol{v} = 0. \tag{3.16}$$

The above phenomenological theory is based on the assumption that the network stress acts on the polymer and not directly on the solvent. In other words, the stress division between the two components is one-sided. This idea has been extended to more general asymmetric stress division in polymer blends [153, 165], and may be used to understand the mutual diffusion between polymers [153] and to study viscoelastic spinodal decomposition in asymmetric polymer blends [166]. The problem of stress–diffusion coupling or asymmetric stress division is ubiquitous, but it is not well recognized in many other systems such as dense colloidal suspensions, dense microemulsions [126], polymeric liquid crystals [14], or fluids near the glass transition, where the two components are not alike and the viscosity is large.

3.2. Linear theory for shear flow

Helfand and Fredrickson (HF) [149] examined the dynamical coupling in shear to linear order in the composition fluctuations by assuming that the stress fluctuations instantaneously follow the composition fluctuations. Their theory most simply illuminates the mechanism of shear-induced fluctuation enhancement, but it is applicable only at very long wavelengths. Here we present a more general linear theory which is valid over a wider wave-vector region and is still analytically tractable. For simplicity, we first consider the Newtonian regime,

$$S\tau \lesssim 1. \tag{3.17}$$

We shall see that fluctuation enhancement is rather mild in the Newtonian regime, and it can be drastic in the non-Newtonian regime, $S\tau \gtrsim 1$. Interestingly, such effects become apparent even when S is still much smaller than the diffusion rate:

$$1/\tau_\xi = D_{co}\xi^{-2} \tag{3.18}$$

over the correlation length ξ. That is,

$$S\tau_\xi \ll 1. \tag{3.19}$$

The definition of the cooperative diffusion constant D_{co} will appear in (3.28) below. We have $\tau_\xi \ll \tau$ except very close to the critical point. In this subsection, the temperature region is assumed to be above the coexistence curve, where phase separation does not occur without shear.

We linearize (3.13) around a homogeneous state under shear flow. To this end we need to know a linear expression for $\overleftrightarrow{\boldsymbol{\sigma}}_p$. When the timescale of the deformations under consideration is much longer than the stress relaxation time τ, it is expressed in terms of the gradient of the polymer velocity $\boldsymbol{v}_p$ as [152, 153]

$$\sigma_{pij} \cong \eta(\phi)\left[\frac{\partial}{\partial x_j}v_{pi} + \frac{\partial}{\partial x_i}v_{pj} - \frac{2}{3}\delta_{ij}\boldsymbol{\nabla}\cdot\boldsymbol{v}_p\right] \tag{3.20}$$

where η is the (zero-shear) viscosity of the solution, strongly dependent on ϕ. For simplicity we have made σ_{pij} traceless by subtracting the last term in (3.20) on the assumption that isotropic expansion or shrinkage of the network takes place on a timescale shorter than that of shear deformations τ. However, this assumption is problematic. In fact, they can occur on the same timescale in gels. We here adopt (3.20) to make the theory as simple as possible. In addition, we have neglected the normal-stress differences N_1 and N_2, which should not be negligible for $S\tau \gtrsim 1$.

It is not trivial that the polymer velocity $\boldsymbol{v}_p$ appears in the constitutive relation (3.20), which was first explicitly stated by Doi [152]. If $\boldsymbol{v}$ or $\boldsymbol{v}_s$ were used instead of $\boldsymbol{v}_p$, we would reach very different conclusions [153]. For example, the dynamical structure factor would become inconsistent with the Brochard–de Gennes form [161], and the kinetic coefficient would not be modified as in (3.31) below. The key relation arising from using $\boldsymbol{v}_p$ is that, in the linear order, $\boldsymbol{\nabla}\cdot\boldsymbol{v}_p$ is related to the time derivative of the deviation $\delta\phi$ as

$$\left(\frac{\partial}{\partial t}+Sy\,\frac{\partial}{\partial x}\right)\delta\phi \cong -\phi\boldsymbol{\nabla}\cdot\boldsymbol{v}_p. \tag{3.21}$$

Then we find

$$\boldsymbol{\nabla}\cdot\boldsymbol{\nabla}\cdot\overleftrightarrow{\boldsymbol{\sigma}}_p \cong -\frac{4\eta}{3\phi}\,\nabla^2\left(\frac{\partial}{\partial t}+Sy\,\frac{\partial}{\partial x}\right)\delta\phi + 2S\eta'\,\frac{\partial^2}{\partial x\,\partial y}\delta\phi \tag{3.22}$$

in terms of $\delta\phi$. The first term arises from the space dependence of the gradient of $\boldsymbol{v}_p$, and the second term from the ϕ-dependence of $\eta(\phi)$, where

$$\eta' = \partial\eta/\partial\phi \sim 6\eta/\phi. \tag{3.23}$$

Rheological data showed that $\eta \propto N^{3.4}\phi^a$ with $a \sim 6$ for semidilute solutions in theta solvent [170, 171]. In the HF theory, the fluctuations of the velocity gradient are neglected, and the first term of (3.22) is absent.

Substitution of (3.22) into (3.13) yields a linear equation for $\delta\phi$ of the form

$$(1-\xi_{ve}^2\,\nabla^2)\left(\frac{\partial}{\partial t}+Sy\,\frac{\partial}{\partial x}\right)\delta\phi = L\left[\nabla^2(r_0 - C\,\nabla^2) - \frac{2}{\phi}\eta' S\,\frac{\partial^2}{\partial x\,\partial y}\right]\delta\phi \tag{3.24}$$

where

$$\delta F/\delta\phi = (r_0 - C\,\nabla^2)\delta\phi \tag{3.25}$$

to linear order in $\delta\phi$. The coefficient r_0 is related to the bulk osmotic modulus K_{os} by

$$K_{os} = \phi^2 r_0. \tag{3.26}$$

The thermal correlation length is thus

$$\xi = (C/r_0)^{1/2} \tag{3.27}$$

and the so-called cooperative diffusion constant D_{co} is of the form

$$D_{co} = Lr_0 = K_{os}/\zeta \sim k_B T/6\pi\eta_0\xi \tag{3.28}$$

which is the diffusion constant not affected by entanglement, and measurable by means of dynamical light scattering at long wavelengths ($q \ll \xi_{ve}^{-1}$, where ξ_{ve} will be determined in (3.32) below). The scaling theory indicates $C \propto 1/\phi$ and $\xi \sim b/\phi$ in the semidilute region.

The Fourier transformation of (3.24) yields a simpler equation for the Fourier component $\phi_{\boldsymbol{q}}$. As in (2.15), we also add a random source term $\theta_{R\boldsymbol{q}}$ on the right-hand side to obtain

$$\left(\frac{\partial}{\partial t} - Sq_x\,\frac{\partial}{\partial q_y}\right)\phi_{\boldsymbol{q}} = -L_{eff}(q)\left[q^2(r_0 + Cq^2) - \frac{2\eta'}{\phi}Sq_xq_y\right]\phi_{\boldsymbol{q}} + \theta_{R\boldsymbol{q}} \tag{3.29}$$

with

$$\langle \theta_{Rq}(t)\theta_{Rq'}(t')\rangle = 2(2\pi)^d \delta(\boldsymbol{q}+\boldsymbol{q}')L_{eff}(q)q^2\delta(t-t'). \tag{3.30}$$

The noise is assumed to be unaffected by shear, and to ensure the Ornstein–Zernike structure factor $I_{OZ}(q) = 1/[r_0 + Cq^2]$ in equilibrium. The kinetic coefficient is modified as follows:

$$L_{eff}(q) = L/[1+\xi_{ve}^2 q^2] \tag{3.31}$$

where ξ_{ve} is defined by

$$\xi_{ve} = \left(\frac{4}{3}L\eta\right)^{1/2} \Big/ \phi = \left(\frac{4}{3}D_{co}\eta/K_{os}\right)^{1/2}. \tag{3.32}$$

If use is made of the estimate (3.14), we have $\xi_{ve} \sim \xi(\eta/\eta_0)^{1/2} \gg \xi$, and find that ξ_{ve} can be very long with increasing ϕ. We notice that the diffusion takes place to achieve viscoelastic stress balance ($\boldsymbol{\nabla}\cdot \overleftrightarrow{\boldsymbol{\sigma}} \to 0$) on spatial scales shorter than ξ_{ve}. We should mention that this length was first introduced by Brochard and de Gennes [172] for semidilute solutions with a good solvent via $\xi_{ve} = (D_{co}\tau)^{1/2}$, where D_{co} is the cooperative diffusion constant and ξ is the correlation length (∼the blob size) in a good solvent. This definition indicates that the usual diffusion is faster than the stress relaxation on spatial scales shorter than ξ_{ve}. A similar viscoelastic length was also introduced for asymmetric polymer blends [153], where it plays an important role in dynamical scattering and phase separation [165, 166]. In fact, strong q-dependence of the kinetic coefficient consistent with (3.31) has been observed for asymmetric polymer blends in their early-stage spinodal decomposition [173].

Equation (3.29) shows that the composition fluctuations are convected by shear flow, and relax with the modified relaxation rate:

$$\Gamma_{eff}(\boldsymbol{q}) = L\left[q^2(r_0+Cq^2) - \frac{2\eta'}{\phi}Sq_xq_y\right] \Big/ [1+\xi_{ve}^2q^2]. \tag{3.33}$$

The equation for the steady structure factor $I(\boldsymbol{q})$ is obtained from (2.17) if $\Gamma(q)$ and L_0 are replaced by $\Gamma_{eff}(\boldsymbol{q})$ and $L_{eff}(q)$, respectively. It depends on S through the S-dependence of $\Gamma_{eff}(\boldsymbol{q})$ as well as that of the convection. If we expand $I(\boldsymbol{q})$ in powers of S as in (2.18), we obtain for $q\xi \ll 1$

$$I(\boldsymbol{q})/I_{OZ}(q) = 1 + 2q_xq_y[\eta' L_{eff}(q)/\phi - \xi^2]S/\,\Gamma_{eff}(\boldsymbol{q}) + \cdots. \tag{3.34}$$

Comparing this with (2.18), we find a surprising result even in the linear order. That is, the correction due to the viscoelasticity is much larger than and has a sign opposite to that due to the convection, in accord with a light scattering experiment performed by Wu *et al* [142] at small shear, $S\tau < 1$. The ratio of these contributions is about $-5(\xi_{ve}/\xi)^2$ for $q\xi_{ve} < 1$ in the present approximation. (A more reliable expansion form of $I(\boldsymbol{q})$ can be found in reference [153].) This suggests that the composition fluctuations are aligned perpendicularly to the flow direction, which is opposite to the case for near-critical fluids. Similar abnormal alignment perpendicular to the stretched direction has been observed in heterogeneous gels [157].

As in (2.19), the integral form of $I(\boldsymbol{q})$ is given by

$$I(\boldsymbol{q}) = \int_0^\infty \mathrm{d}t\ \exp\left[-2\int_0^t \mathrm{d}t_1\ \Gamma_{eff}(\boldsymbol{q}(t_1))\right] 2L_{eff}(|\boldsymbol{q}(t)|)\boldsymbol{q}(t)^2 \tag{3.35}$$

where $\boldsymbol{q}(t) = \boldsymbol{q} + St q_x \boldsymbol{e}_y$ as in (2.20). It is important that $\Gamma_{eff}(\boldsymbol{q})$ can be negative even for positive r_0 for $S > S_c$, indicating growth of the fluctuations. The critical shear rate S_c is given by

$$S_c = r_0\phi/\eta' \cong K_{os}/6\eta \tag{3.36}$$

where use has been made of (3.23) and (3.26). To examine the growth in more detail, we define two parameters:

$$\delta = S/S_c - 1 \tag{3.37}$$

$$M = (\xi_{ve}/\xi)^2 \sim \tau/\tau_\xi \gg 1. \tag{3.38}$$

For simplicity, we assume $0 < \delta \lesssim 1$. Some calculations show that the maximum of $-\Gamma_{eff}(\boldsymbol{q})$ is attained at $q_x = q_y = \pm q_m$ and $q_z = 0$, with

$$q_m^2 = \xi^{-2}\delta\big/[\sqrt{1+M\delta}+1] \tag{3.39}$$

and is equal to

$$\Gamma_{max} = D_{co}\xi^2 q_m^4. \tag{3.40}$$

In particular, for $\delta \gg 1/M$, we obtain

$$q_m \cong \xi^{-1}(\delta/M)^{1/4} \cong \delta^{1/4}/(\xi\xi_{ve})^{1/2} \tag{3.41}$$

$$\Gamma_{max} \cong \frac{3}{4}(K_{os}/\eta)\delta. \tag{3.42}$$

However, the growth is transient, because $\Gamma_{eff}(\boldsymbol{q})$ is negative only in the narrow region where $q \lesssim \delta^{1/2}\xi^{-1}$, and the convection brings the wave vector outside this unstable region. The duration time t^* of the growth is of order $\delta^{1/2}/S$, and the peak height I_{max} of $I(\boldsymbol{q})$ is proportional to the exponential factor $\exp(\Gamma_{max}t^*)$. For $\delta \gg 1/M$, it follows that

$$\log(I_{max}) \cong 2^{-1/2}K_{os}\delta^{3/2}/\eta S \sim 4\delta^{3/2} \tag{3.43}$$

where S in the denominator has been replaced by S_c, and use has been made of (3.36). It is certain that the enhancement is large for $\delta \gtrsim 1$, though our calculation is not applicable for $\delta \gg 1$. For $\delta < 1/M \ll 1$, the volume of the unstable wave-vector region is very narrow, and $\Gamma_{max}t^* \ll 1$, leading to no significant exponential growth. Obviously, our linear theory can be used only when the fluctuation enhancement is weak, and a nonlinear theory is needed to study the strongly enhanced regime.

In setting up (3.20), we have assumed that the timescale of the composition fluctuations is longer than τ. Here we confirm that the maximum growth rate Γ_{max} given in (3.42) is certainly smaller than $1/\tau$ if $K_{os}\delta < G$, where $G = \eta/\tau$ is the shear modulus. We also note that the q-dependence of the modified kinetic coefficient $L_{eff}(q)$ in (3.31), which is neglected in the HF theory, is crucial in the above calculation.

3.3. The normal-stress effect, and the non-Newtonian regime

In the previous subsection we have neglected the normal-stress effect. Because the convection makes the mathematics very complex, let us assume that all of the deviations are varying only in the y- (velocity gradient) direction [151]. We take the long-wavelength limit $q\xi_{ve} \ll 1$ in (3.13) to obtain the equation for the deviation $\delta\phi$:

$$\frac{\partial}{\partial t}\delta\phi = L\,\frac{\partial^2}{\partial y^2}\left[r_0\,\delta\phi - \frac{1}{\phi}\,\delta\sigma_{pyy}\right] \tag{3.44}$$

where $r_0 = K_{os}/\phi^2$ is defined by (3.26), and $\delta\sigma_{pyy}$ is the deviation of the yy-component of the polymer stress. This gives a diffusion constant in the velocity gradient direction given by

$$D_\perp = L[r_0 - (\partial\sigma_{pyy}/\partial\phi)/\phi]. \tag{3.45}$$

Here we take the derivative with respect to ϕ at a fixed shear stress, assuming that $\delta\phi$ changes more slowly than the shear stress deviation. Because $\partial\sigma_{pyy}/\partial\phi \sim N_1/\phi$ in terms of the first normal-stress difference N_1, the fluctuations varying along the y-axis are linearly unstable for $K_{os} < \phi(\partial\sigma_{pyy}/\partial\phi) \sim N_1$ [150]. In polymer solutions, however, the assumption of neglecting fluctuations varying in the flow direction seems to be too restricted, as our simulations will suggest. On the other hand, it may well be used to discuss flow instability of layered structures aligned in the flow direction [176].

For a long time, considerable attention has been paid to migration or diffusion of polymers [177] or colloidal particles [48, 178] in the velocity gradient direction. In particular, Nozières and Quemada [50] proposed the same equation as (3.44) to describe plug flow formation in concentrated colloidal suspensions flowing through a capillary, where the quantity corresponding to $\delta\sigma_{pyy}$ is called a lift force. In a similar manner, we have discussed how a slipping layer consisting of solvent appears at a boundary and grows for a semidilute solution near the coexistence temperature [179].

We have found that light scattering increases when S somewhat exceeds S_c defined by (3.36). However, S_c is of order $1/\tau$ above the coexistence curve, so the enhancement is mild under (3.17) or in the Newtonian regime. We then advance some speculations for the non-Newtonian regime. The dynamical equation (3.13) indicates that the fluctuations grow when the typical value of the shear stress σ_{pxy} or the normal-stress difference N_1 exceeds the osmotic modulus K_{os}. In the rheological literature [174, 175] it is known that

$$\sigma_{pxy} \sim N_1 \sim G(S\tau)^{\beta} \tag{3.46}$$

with $\beta \sim 0.2$ in the non-Newtonian regime. The condition of strong fluctuation enhancement will be given by

$$G(S\tau)^{\beta} \gtrsim K_{os} \quad \text{or} \quad (S\tau)^{\beta} \gtrsim (T - T_{sp})/(T_{cx} - T_{sp}) \tag{3.47}$$

where T_{sp} is the spinodal temperature and T_{cx} is the coexistence temperature. The above condition can also be obtained from (3.44) or (3.45) if (3.46) is used. Thus enhancement is not expected in a good solvent where $K_{os} \gg G$, whereas it emerges noticeably as the temperature approaches the coexistence curve where $K_{os} \sim G$.

Rangel-Nafaile *et al* [138] developed a thermodynamic theory of shear-induced phase separation, and claimed that their theory is in good agreement with experiments. They assumed that the total free energy consists of the Flory–Huggins free energy and a stored elastic energy f_{el} of the order of N_1. Such a form of the free energy was suggested by Marrucci's work [180] on the dumb-bell model. Then the spinodal was determined from

$$K_{os} + \phi^2(\partial^2 f_{el}/\partial\phi^2) = 0 \tag{3.48}$$

where the derivative with respect to ϕ was performed with the shear stress held fixed. However, the second derivative of f_{el} is positive, leading to a downward shift of the spinodal if ϕ is much larger than a critical entanglement volume fraction ϕ^*. They hence claimed that an upward shift of the spinodal is expected for $\phi \sim \phi^*$. Similar approaches have been taken also by other authors [181, 182]. In contrast, if the problem is treated dynamically as in recent theories, the apparent shift due to the stress–diffusion coupling is definitely upward. Apart from the sign, the absolute value of the shift from the thermodynamic assumptions can be consistent with (3.47) in the non-Newtonian regime.

We believe that it is appropriate to introduce the concept of the stored free energy or the elastic free energy to adequately describe viscoelastic fluids. In the thermodynamic theory, however, Rangel-Nafaile *et al* have followed the usual thermodynamics, not explicitly examining space-dependent fluctuations, in contrast to the recent theories on polymer solutions and those on gels. Jou *et al* [182] stressed that thermodynamic arguments, if

improved, can be useful in understanding shear effects in polymers, in view of the still weak predicting power of the dynamical theory.

3.4. Time-dependent Ginzburg–Landau theory

3.4.1. Conformation and stress tensors. In the phase transition of polymer solutions, the order parameter is the polymer volume fraction ϕ. In describing viscoelastic effects on the composition inhomogeneities, it is convenient to introduce a new dynamical variable $\overleftrightarrow{\mathbf{W}} = \{W_{ij}\}$, which is a symmetric tensor representing chain conformations undergoing deformations. Note that ϕ changes more rapidly than $\overleftrightarrow{\mathbf{W}}$ even at relatively small wavenumbers for highly entangled systems. We need to construct a canonical form of the dynamical equations, or a set of Langevin equations satisfying the fluctuation-dissipation relations [150, 151], which is the traditional approach in critical dynamics [9, 10]. We should mention that such formal frameworks for viscoelastic fluids have already been presented, but without discussions of phase transitions [183, 184].

In the semidilute regime we may define $\overleftrightarrow{\mathbf{W}}$ as follows. Let us consider entanglement points $\boldsymbol{R}_n$ on a chain, and number them consecutively along it as $n = 1, 2, \ldots, N/N_e$, where N/N_e is the number of entanglements on a chain. Then W_{ij} may be defined as

$$W_{ij} = \frac{1}{Nb^2}\left\langle \sum_n (\boldsymbol{R}_{n+1} - \boldsymbol{R}_n)_i (\boldsymbol{R}_{n+1} - \boldsymbol{R}_n)_j \right\rangle_{\text{chain}}. \tag{3.49}$$

Here b is the monomer size, the sum is taken over entanglement points on a chain, and the average $\langle \cdots \rangle_{\text{chain}}$ is taken over all chains contained in a volume element whose linear dimension is of the order of the gyration radius ($\sim N^{1/2}b$). In equilibrium, we assume the Gaussian distribution of $\boldsymbol{R}_{n+1} - \boldsymbol{R}_n$ to obtain $\langle W_{ij} \rangle_{eq} = \delta_{ij}$, where $\langle \cdots \rangle_{eq}$ is the equilibrium average.

The free energy due to the fluctuations of ϕ and $\overleftrightarrow{\mathbf{W}}$ is written as

$$F\{\phi, \overleftrightarrow{\mathbf{W}}\} = \int \mathrm{d}\boldsymbol{r} \left[f + \frac{1}{2} C |\boldsymbol{\nabla}\phi|^2 + \frac{1}{4} G Q(\overleftrightarrow{\mathbf{W}}) \right]. \tag{3.50}$$

f is the Flory–Huggins free-energy density [13], given by

$$f \cong (k_B T/v_0)\left[\frac{\phi}{N} \ln \phi + \left(\frac{1}{2} - \chi \right)\phi^2 + \frac{1}{6}\phi^3 \right] \tag{3.51}$$

where v_0 is the volume of a monomer, and χ is the so-called interaction parameter, dependent on the temperature T. The osmotic bulk modulus $K_{os} = r_0 \phi^2$ introduced in (3.26) is expressed as

$$K_{os} = (k_B T/v_0)\phi^2 \left[\phi + (1 - 2\chi) + \frac{1}{N\phi} \right]. \tag{3.52}$$

In the gradient free energy, the coefficient C may be determined using the random-phase approximation [13] as

$$C = (k_B T/v_0) b^2/18\phi. \tag{3.53}$$

The relation $C \propto 1/\phi$ is important in the semidilute regime. G is the shear modulus, given by

$$G \sim (k_B T/v_0)\phi^{\alpha}. \tag{3.54}$$

Simple scaling arguments showed that $\alpha = 3$, whereas experiments indicated that $\alpha \cong 2.25$ in theta solvents [170, 171]. $Q(\overleftrightarrow{\mathbf{W}})$ is assumed to be of the simplest Gaussian form:

$$Q(\overleftrightarrow{\mathbf{W}}) = \sum_{ij} (W_{ij} - \delta_{ij})^2 \tag{3.55}$$

which is questionable for large deformations [174, 175], but we will use (3.55) for mathematical simplicity.

At the starting point of our theory, the gross variables that we consider are ϕ, $\overleftrightarrow{\mathbf{W}}$, the mass-density deviation $\delta\rho$, the relative velocity $\boldsymbol{w}$, and the average velocity $\boldsymbol{v}$. The polymer velocity is $\boldsymbol{v}_p = \boldsymbol{v} + \boldsymbol{w}$. The total free energy is of the form

$$\mathcal{F} = F\{\phi, \overleftrightarrow{\mathbf{W}}\} + \frac{1}{2}\int \mathrm{d}\boldsymbol{r} \left[\frac{1}{B}(\delta\rho)^2 + \bar{\rho}\boldsymbol{v}^2 + \bar{\rho}\phi\boldsymbol{w}^2\right] \tag{3.56}$$

where $B = \rho(\partial\rho/\partial p)_T$ is the compressibility multiplied by ρ^2 and is very small, and use has been made of the relation $\rho_p \boldsymbol{v}_p^2 + \rho_s \boldsymbol{v}_s^2 \cong \bar{\rho}\boldsymbol{v}^2 + \bar{\rho}\phi\boldsymbol{w}^2$.

Because $\overleftrightarrow{\mathbf{W}}$ represents the network deformation, its motion is determined by the polymer velocity $\boldsymbol{v}_p$, and its simplest dynamical equation is of the form

$$\frac{\partial}{\partial t} W_{ij} + (\boldsymbol{v}_p \cdot \boldsymbol{\nabla}) W_{ij} - \sum_k (D_{ik} W_{kj} + W_{ik} D_{jk}) = -\frac{1}{\tau}(W_{ij} - \delta_{ij}) \tag{3.57}$$

where D_{ij} is the gradient of the polymer velocity

$$D_{ij} = \frac{\partial}{\partial x_j} v_{pi}. \tag{3.58}$$

The left-hand side of (3.57) is called the upper convective time derivative in the rheological literature [174, 175]. We choose it because of its simplicity, though there can be a class of choices which satisfy the requirement of the frame invariance. τ on the right-hand side is the stress relaxation time, which is very long in the semidilute region. Once we have the free energy and the dynamical equation for $\overleftrightarrow{\mathbf{W}}$, we may calculate the network stress tensor induced by $\overleftrightarrow{\mathbf{W}}$ as follows:

$$\overleftrightarrow{\boldsymbol{\sigma}}_p = G\,\overleftrightarrow{\mathbf{W}} \cdot (\overleftrightarrow{\mathbf{W}} - \overleftrightarrow{\mathbf{I}}) + \frac{1}{4} G Q\,\overleftrightarrow{\mathbf{I}}\,. \tag{3.59}$$

See appendix A for its derivation. The total stress tensor is expressed as

$$\overleftrightarrow{\boldsymbol{\Pi}} = \left[\frac{\bar{\rho}}{B}\delta\rho - f + \frac{C}{2}|\boldsymbol{\nabla}\phi|^2\right]\overleftrightarrow{\mathbf{I}} + C(\boldsymbol{\nabla}\phi)(\boldsymbol{\nabla}\phi) - \overleftrightarrow{\boldsymbol{\sigma}}_p - \overleftrightarrow{\boldsymbol{\sigma}}_{vis}\,. \tag{3.60}$$

The first term is the diagonal part, $\overleftrightarrow{\mathbf{I}} = \{\delta_{ij}\}$ being the unit tensor, and the last term represents the viscous stress tensor arising from the solvent viscosity η_0. The divergence of $\overleftrightarrow{\boldsymbol{\Pi}}$ is of the form

$$\boldsymbol{\nabla} \cdot \overleftrightarrow{\boldsymbol{\Pi}} = \frac{\bar{\rho}}{B}\boldsymbol{\nabla}\delta\rho - \frac{\delta F}{\delta\phi}\boldsymbol{\nabla}\phi + \frac{1}{4} Q\,\boldsymbol{\nabla} G - \boldsymbol{\nabla} \cdot \overleftrightarrow{\boldsymbol{\sigma}}_p - \eta_0 \nabla^2 \boldsymbol{v}. \tag{3.61}$$

3.4.2. Chemical potentials. So far we have not taken the incompressible limit $B \to 0$. This is just because we need to obtain unambiguous expressions for μ_p and μ_s as given below. In addition, before this limit is taken, we may naturally introduce the osmotic pressure $\pi(\phi, T)$ as the pressure difference of a polymer solution and a solvent separated by a semi-permeable membrane, which will be derived in appendix B.

We define the chemical potentials μ_p and μ_s appearing in (3.7) and (3.8) in our Ginzburg–Landau scheme by

$$\mu_p = \frac{\delta}{\delta \rho_p}\mathcal{F} \cong \frac{1}{B}\,\delta\rho + \frac{1-\phi}{\rho}\frac{\delta F}{\delta \phi} \tag{3.62}$$

$$\mu_s = \frac{\delta}{\delta \rho_s}\mathcal{F} \cong \frac{1}{B}\,\delta\rho - \frac{\phi}{\rho}\frac{\delta F}{\delta \phi}. \tag{3.63}$$

We fix ρ_s (or ρ_p) and $\overleftrightarrow{\mathbf{W}}$ in the derivative of $\mathcal{F}$ with respect to ρ_p (or ρ_s), while we fix ρ and $\overleftrightarrow{\mathbf{W}}$ in the derivative with respect to ϕ. Therefore, the chemical potential difference is certainly given by (3.12), and

$$\rho_p\,\boldsymbol{\nabla}\mu_p + \rho_s\,\boldsymbol{\nabla}\mu_s \cong \frac{1}{B}\bar{\rho}\,\boldsymbol{\nabla}\delta\rho - \frac{\delta F}{\delta \phi}\,\boldsymbol{\nabla}\phi. \tag{3.64}$$

From (3.15) and (3.61), $\boldsymbol{F}_p$ is obtained as

$$\boldsymbol{F}_p = -\frac{1}{4}Q\,\boldsymbol{\nabla}G + \boldsymbol{\nabla}\cdot\overleftrightarrow{\boldsymbol{\sigma}}_p\,. \tag{3.65}$$

The first term ($\propto \boldsymbol{\nabla}G$) has arisen from the composition dependence of G (and is not included in (3.13)).

3.4.3. Langevin equations. We have obtained a closed set of dynamical equations for the gross variables. We then add three Gaussian noise terms on the right-hand sides of (3.10), (3.15), and (3.57) as in the case of near-critical fluids. The amplitudes of the noise terms are determined from the fluctuation-dissipation relations. The thermal fluctuations created by the noise terms are indispensable in the shear effects above the coexistence curve. Recall that $I(\boldsymbol{q})$ in (3.35) has arisen from the thermal noise. To make the equations as simple as possible, we here set up the Langevin equations in two limits. In the incompressible limit, $\delta\rho$, B, and $\boldsymbol{\nabla}\cdot\boldsymbol{v}$ tend to zero, while the pressure deviation $\delta p = \bar{\rho}\,\delta\rho/B$ remains finite. In the adiabatic limit we set $\partial\boldsymbol{v}/\partial t = \partial\boldsymbol{w}/\partial t = 0$ in their dynamical equations, as in the Kawasaki limit (2.7) for near-critical fluids.

First, from (3.11), $\boldsymbol{w}$ is expressed as

$$\boldsymbol{w} = \frac{1}{\zeta}\Big[-\phi\,\boldsymbol{\nabla}\frac{\delta F}{\delta \phi} + \boldsymbol{F}_p\Big] + \boldsymbol{w}_R. \tag{3.66}$$

where $\boldsymbol{F}_p$ is given by (3.65). The random relative velocity $\boldsymbol{w}_R$ is characterized by

$$\langle \boldsymbol{w}_R(\boldsymbol{r}, t)\boldsymbol{w}_R(\boldsymbol{r}', t')\rangle = -2(k_B T/\zeta)\,\nabla^2\delta(\boldsymbol{r}-\boldsymbol{r}')\,\delta(t-t')\,\overleftrightarrow{\mathbf{I}}\,. \tag{3.67}$$

Second, $\boldsymbol{v}$ is determined by

$$-\eta_0\,\nabla^2\boldsymbol{v} = \Big[-\phi\,\boldsymbol{\nabla}\frac{\delta F}{\delta \phi} + \boldsymbol{F}_p + \boldsymbol{\zeta}_R\Big]_\perp \tag{3.68}$$

where $[\cdots]_\perp$ denotes taking the transverse part. The random force density $\boldsymbol{\zeta}_R$ satisfies (2.6), as for near-critical fluids. Third, we add a noise term on the right-hand side of (3.57):

$$\frac{\partial}{\partial t}W_{ij} + (\boldsymbol{v}_p\cdot\boldsymbol{\nabla})W_{ij} - \sum_k (D_{ik}W_{kj} + W_{ik}D_{jk}) = -\frac{1}{\tau}(W_{ij}-\delta_{ij}) + f_{Rij} \tag{3.69}$$

where

$$\langle f_{Rij}(\boldsymbol{r},t)\, f_{Rk\ell}(\boldsymbol{r}',t')\rangle = 2(K_BT/\tau G)(\delta_{ik}\delta_{j\ell}+\delta_{i\ell}\delta_{jk})\delta(\boldsymbol{r}-\boldsymbol{r}')\delta(t-t'). \tag{3.70}$$

At this stage, $\boldsymbol{w}$ and $\boldsymbol{v}$ have been expressed (or slaved) by ϕ and $\overleftrightarrow{\mathbf{W}}$, so the independent dynamical variables are now ϕ and $\overleftrightarrow{\mathbf{W}}$.

3.4.4. Linear coupled equations. The Langevin equations obtained are so complex that we can treat only their linearized versions in analytic work, in which the deviation $\delta\phi$ is coupled to $Z = \boldsymbol{\nabla}\cdot\boldsymbol{\nabla}\cdot\overleftrightarrow{\mathbf{W}}$. Their Fourier components are governed by

$$\left(\frac{\partial}{\partial t} - Sq_x\frac{\partial}{\partial q_y}\right)\phi_{\boldsymbol{q}} = -L[q^2(r_0+Cq^2) - (2G'/\phi)\tau Sq_xq_y]\phi_{\boldsymbol{q}} - (LG/\phi)Z_{\boldsymbol{q}} + \theta_{R\boldsymbol{q}} \tag{3.71}$$

$$\left(\frac{\partial}{\partial t} - Sq_x\frac{\partial}{\partial q_y}\right)\left[Z_{\boldsymbol{q}} - (2q^2/\phi)\phi_{\boldsymbol{q}}\right] = -\frac{1}{\tau}Z_{\boldsymbol{q}} - (2S\tau'/\tau)q_xq_y\phi_{\boldsymbol{q}} + f_{R\boldsymbol{q}} \tag{3.72}$$

where $G' = \partial G/\partial\phi$, $\tau' = \partial\tau/\partial\phi$, and the terms higher than S^2 are omitted. The random forces $\theta_{R\boldsymbol{q}}$ and $f_{R\boldsymbol{q}}$ are the Fourier transforms of $-\phi\,\boldsymbol{\nabla}\cdot\boldsymbol{w}_R$ and $\boldsymbol{\nabla}\cdot\boldsymbol{\nabla}\cdot\overleftrightarrow{\mathbf{f}}_R$, respectively. We notice that our previous linear equation (3.29) naturally follows from (3.71) and (3.72) when the timescale of $\phi_{\boldsymbol{q}}$ is much longer than τ. The coupling of the two variables becomes stronger with increasing G/K_{os}. They relax almost independently in a good solvent, where G/K_{os} is typically of order 0.01. However, at the theta temperature $T = T_\theta$ (or at $\chi = 1/2$), G/K_{os} is known to be of order 1 [170, 171].

Without shear, these equations may be used to calculate the dynamical structure factor in one-phase states ($r_0 > 0$) [153, 161], and early-stage spinodal decomposition in unstable states ($r_0 < 0$) [166]. Transient relaxation after cessation of shear can also be studied [163, 164]. In the presence of shear, they have been used to calculate the steady-state structure factor $I(\boldsymbol{q})$. Here there arises a 2×2 matrix equation involving the convection operator $Sq_x\,\partial/\partial q_y$, so solving it analytically is still difficult. In a first attempt, only the correction linear in S to $I(\boldsymbol{q})$ was calculated [153] (see a comment below (3.34)). Then the equation was solved numerically in the $\boldsymbol{q}$-space by Milner [154] and by Ji and Helfand [155], in qualitative agreement with experiments in the case of mild fluctuation enhancement [142]. It goes without saying that the linear theory is not applicable to regimes of strong fluctuation enhancement with non-Newtonian shear [143, 145], or below the coexistence temperature.

3.5. Simulation of shear-induced phase separation

Recently we have solved our Langevin equations numerically for shear flow in two space dimensions [156]. They have also been solved without shear to simulate deeply quenched polymer solutions [185]. In this article, we choose somewhat different values of the parameters and show results for non-Newtonian cases and below the coexistence curve. In our scheme, ϕ obeys (3.4), where $\boldsymbol{w}$ is given by (3.66), $\boldsymbol{F}_p$ being given by (3.65). On the other hand, $\overleftrightarrow{\mathbf{W}}$ obeys (3.69). In calculating the average velocity $\boldsymbol{v}$ determined from (3.68), we use a new computer scheme which enables the FFT (fast-Fourier-transform) method to be carried out for shear flow [186]. We integrate the Langevin equations on a 128×128 square lattice, by applying steady shear at $t = 0$. The space and time are measured in units of $\ell = b(N/72)^{1/2}$ and $\tau_0 = (\phi^2/\zeta)k_BT/(v_0N^{1/2}\ell^2)$, where (3.53) is

assumed and ϕ^2/ζ is independent of ϕ from (3.9). Let us consider a one-phase state in which

$$\langle\phi\rangle = 2\phi_c = 2N^{-1/2} \tag{3.73a}$$

where

$$T = T_c \qquad \text{or} \qquad u = N^{1/2}(2\chi - 1) = 2. \tag{3.73b}$$

For this state, we may express the correlation length ξ, the cooperative diffusion constant D_{co}, and the viscoelastic length ξ_{ve} as $\xi = 2\ell$ from (3.27), $D_{co} = \ell^2/2\tau_0$ from (3.28), and $\xi_{ve} = 68^{1/2}\ell = 17^{1/2}\xi$ from (3.32). The shear modulus is assumed to be of the form $G = (k_BT/v_0)\phi^3$ from (3.54), leading to $K_{os}/G = 1 - u(\phi_c/\phi) + (\phi_c/\phi)^2$, where u is defined by (3.73*b*). Then K_{os}/G is 0.25 in the reference state (3.73) and 1.25 for the theta condition $u = 0$. We furthermore set $\zeta = 18\eta_0\phi^2/b^2$ from (3.9). The stress relaxation time τ will be assumed to be dependent on ϕ and Q, as follows:

$$\tau = \tau_0[(\phi/\phi_c)^4 + 1]/(1 + Q) \tag{3.74}$$

where Q is defined by (3.55). In reference [156] we have set $\tau = 0.3\tau_0[(\phi/\phi_c)^4 + 1]$, so τ is longer here. Then in a homogeneous state, the zero-shear viscosity due to deformations is

$$\eta_p = \frac{1}{4}\eta_0(\phi/\phi_c)^3[(\phi/\phi_c)^4 + 1] \tag{3.75}$$

and is equal to $34\eta_0$ in the reference state (3.73). On the other hand, in a homogeneous state under strong shear, $S\tau \gg 1$, we solve (3.57) to obtain asymptotic nonlinear relations:

$$\sigma_{pxy} \sim S^{3/5} \qquad \sigma_{pxx} - \sigma_{pyy} \sim S^{4/5} \tag{3.76}$$

where $Q \gg 1$ in (3.74). We have thus introduced non-Newtonian behaviour simply from the factor $1/(1 + Q)$ in τ, with the Gaussian form of the elastic free energy unchanged, though this is not the traditional approach [174, 175, 155].

We make the dynamical equations dimensionless, but there remains a parameter $\epsilon = [v_0N^{3/2}/\ell^d]^{1/2}$, which has not yet been specified, d being the spatial dimensionality. It represents the noise strength, and our model is self-consistent for arbitrary ϵ, so we set $\epsilon = 0.1$ in our simulations. In an initial stage after application of shear, thermal fluctuations begin to grow with wave vectors markedly aligned in the abnormal direction ($q_x \sim q_y$). If $S\tau$ is small, their growth stops at a certain level, giving rise to the abnormal structure factor observed [142] and calculated in the linear theories. The elongated directions of the fluctuations are opposite to those in near-critical fluids. If $S\tau \gtrsim 1$, the fluctuations gradually grow and coarsen into larger length scales. Eventually, there arises a dynamical steady state with much enhanced fluctuations, as previously reported [156].

In figure 4, we show snapshots of the composition fluctuations $\phi(x, y, t)/\phi_c$ for $S\tau_0 = 0.05$ and 0.1 at $t = 120$ in the state (3.73). The maximum and minimum of $\phi(x, y, t)/\phi_c$ are 3.32 and 0.24 for $S\tau_0 = 0.05$, and are 3.78 and 0.095 for $S\tau_0 = 0.1$. The amplitude of the structure factor here is comparable to that in usual spinodal decomposition without shear. We can see very complicated fluctuations with various spatial scales being continuously deformed by shear. Comparing the two cases, we find that they become finer and sharper with increasing shear. For the case where $S\tau_0 = 0.1$, the polymer-rich regions apparently form a network connected throughout the system. In our previous work [156], we have shown similar snapshots with smaller τ. The structure factor is fluctuating in time because of the finite-system-size effect. Its time averages qualitatively resemble but much exceed those in the previously obtained scattering pattern in the q_x–q_y plane [142].

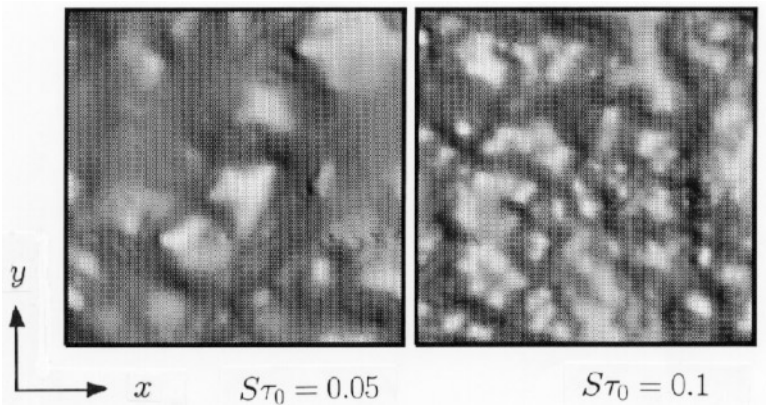

Figure 4. $\phi(x, y, t)/\phi_c$ for $S\tau_0 = 0.05$ and 0.1 at $t = 120$, above the coexistence curve. At this time, the system is in a dynamical steady state with strong fluctuations being deformed by shear on the timescale of $1/S$. The system length is 128. The space and time are measured in units of $\ell = \xi/2$ and $\tau_0 = \ell^2/2D_{co}$, ξ and D_{co} being the correlation length and the cooperative diffusion constant in equilibrium. The x- (horizontal) axis is in the flow direction and the y- (vertical) axis is in the velocity gradient direction.

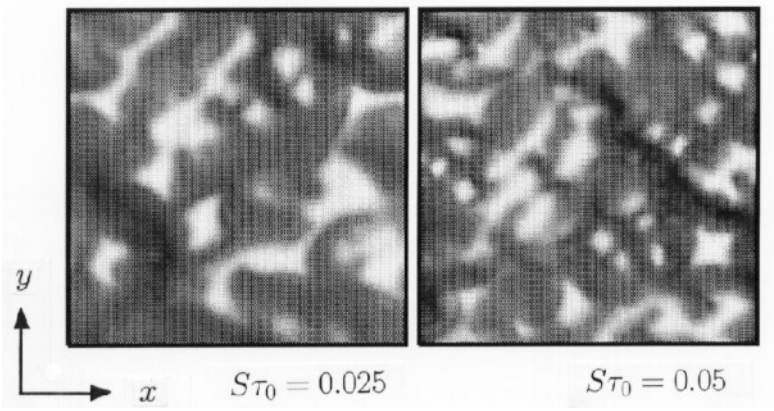

Figure 5. $\phi(x, y, t)/\phi_c$ for $S\tau_0 = 0.025$ and 0.05 at $t = 200$, below the spinodal point. The system is in dynamical steady states, and the solvent-rich regions are finer and more elongated for the larger-shear case. We can also see that the polymer in the solvent-rich rich regions is more dilute than in figure 4. The space and time are measured in the same units as in figure 4.

In figure 5, we show snapshots taken at a lower temperature, with $u = N^{1/2}(2\chi - 1) = 3$, with the same volume fraction $\langle\phi/\phi_c\rangle = 2$, for the two cases where $S\tau_0 = 0.025$ and 0.05 at $t = 200$. The maximum and minimum of $\phi(x, y, t)/\phi_c$ are 3.53 and 0.01 for $S\tau_0 = 0.025$, and are 3.23 and 0.01 for $S\tau_0 = 0.05$. The system is below the classical spinodal point $u \cong 2.5$. Here we observe the formation of sharper interface structures. In the solvent-rich regions, ϕ becomes very small, whereas in the polymer-rich regions, it slowly increases (where deswelling of the solvent is taking place, as in gels). Nevertheless, at relatively large shear the system remains in a two-phase dynamical steady state, without infinite growth of domains. As a marked feature, the solvent-rich regions are narrow and compressed.

But we observe that the system is finally divided into two regions, one mostly with

solvent and the other polymer-rich, at very small shear and for deep quench depth ($S\tau_0 = 0.001$ and $u = 5$, for example). In transient time regions in such cases, solvent-rich regions are very easily deformed by shear into extended shapes, and the shear stress decreases abruptly once such solvent-rich regions are percolated throughout the system. (Recall that a gas droplet in a viscous liquid can be elongated into a slender shape in shear flow [91, 92, 93].) Here, the thin solvent-rich regions should act as a lubricant, serving to diminish the measured viscosity. This picture was originally presented by Wolf and Sezen [187] to interpret their finding of a viscosity decrease which signals the onset of phase separation at small shear in semidilute solutions. These aspects will be studied in more detail in a future paper.

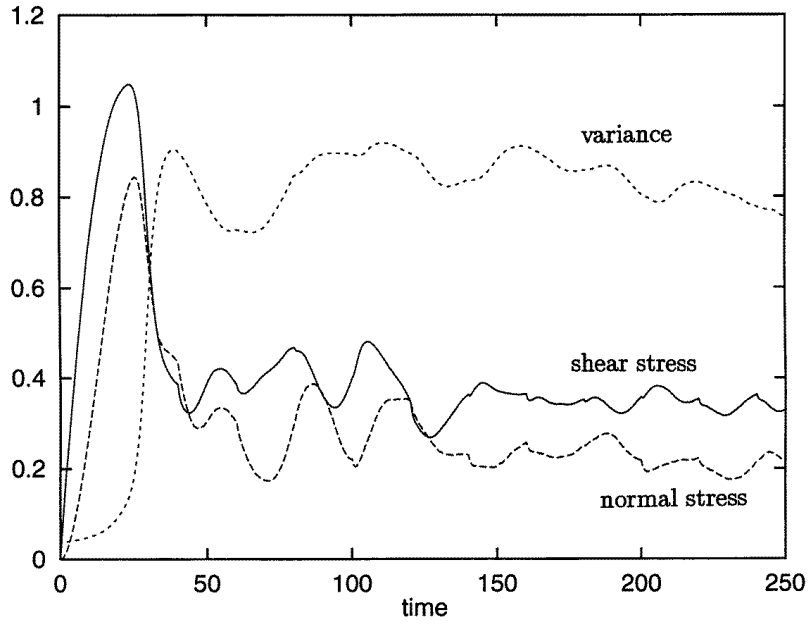

Figure 6. The time evolution of the shear stress, normal-stress difference, and composition variance in dimensionless forms after application of shear. The system is below the spinodal point, and $S\tau_0 = 0.05$ as in the second case of figure 5. The first overshoots of the shear stress and normal-stress difference arise with development of the shear-induced fluctuations. The temporal fluctuations after the second peaks are chaotic.

We next examine the time evolution of the shear stress and the normal-stress difference. They are defined by

$$\sigma_{xy} = \langle \sigma_{pxy} \rangle - \langle C(\phi)(\partial\phi/\partial x)(\partial\phi/\partial y) \rangle$$
$$N_1 = \langle \sigma_{pxx} - \sigma_{pyy} \rangle + \langle C(\phi)[(\partial\phi/\partial y)^2 - (\partial\phi/\partial x)^2] \rangle$$

where the averages are taken over the lattice points. In our cases, the first terms, the viscoelastic contributions, are much larger than the second terms arising from the composition inhomogeneities, while the latter ones are the sole singular contributions in near-critical fluids. In our previous report [156], we have found very strong temporal fluctuations of the stress components in dynamical steady states, above the coexistence curve. In such states the network composed of elongated polymer-rich regions supports most of the stress. Obviously, continuous formation and disruption of the network produces

abnormal fluctuations of the stress. In figure 6, we show these two stress components divided by η_0/τ_0 below the classical spinodal point. The parameters chosen are $u = 3$, $\langle\phi/\phi_c\rangle = 2$, and $S\tau_0 = 0.05$, which are common to the second case of figure 5. Here σ_{xy} and N_1 are considerably more reduced in the two-phase state than in the homogeneous state. (The dimensionless shear stress would reach 1.7, from (3.75), if there were no composition fluctuations.) As a result, their first peaks at $t \sim 20$ look to be more pronounced than in the previous case, above the coexistence curve [156]. Our simulations evidently show that the shear stress and the normal-stress difference begin to decrease with the emergence and growth of the shear-induced fluctuations. (Below the spinodal point, fluctuations grow even without shear, but the timescale is much longer [166].) The first peaks thus created are reproducible over many runs, while the temporal fluctuations after the second peaks are chaotic and not reproducible. In figure 6, we also show the time evolution of the composition variance defined by $[\langle(\phi/\phi_c - 2)^2\rangle]^{1/2}$ taken over all of the lattice points, which increases with the local phase separation.

More than three decades ago, Lodge [5] reported abnormal temporal fluctuations of the normal-stress difference in a hole of 1 mm diameter, from studying polymer solutions contained in a cone–plate apparatus. He ascribed its origin to the growth of inhomogeneities or gel-like particles. Peterlin and Turner [6] suggested temporary network formation in sheared polymer solutions to explain their finding of a maximum in the shear stress after application of shear. In subsequent measurements [141, 188, 144], σ_{xy} and N_1 have exhibited a peak after a relatively short time (the first overshoot), arising from transient stretching of polymer chains [14], and a second peak (the second overshoot), arising from shear-induced phase separation. In our dynamical model, we are neglecting the former relaxation process, so our first overshoots in figure 6 correspond to the observed second overshoots. It would be informative if further rheological experiments were performed at various temperatures, including the case below the spinodal point, or in small spatial regions as in Lodge's case.

4. Summary

In section 1, we have given a brief overview of the current research on fluids undergoing phase transitions in shear flow. In section 2, we have critically reviewed theories and experiments for near-critical fluids, and also discussed other fluids such as polymer solutions or blends in which viscoelasticity is not important. We have examined in some detail the critical temperature shift caused by shear, because it has been one of the main problems in polymer science. The shear effects are particularly interesting in the course of phase separation. In spinodal decomposition, extreme elongation of domains has been observed in the strong-shear regime. In nucleation, the mechanisms of break-up, coagulation, and advection come into play. We are interested in whether or not nucleation is suppressed by the break-up mechanism, and spinodal decomposition remains as a unique route to phase separation. We have also discussed the effects of stirring, gentle or violent, on critical behaviour and phase separation. In section 3, we have treated shear-induced phase separation in semidilute polymer solutions, in which viscoelasticity is crucial. We have explained three major theoretical ingredients, a dynamical stress–diffusion coupling, a viscoelastic Ginzburg–Landau theory, and computer simulations, together with some new analytic and numerical results. Here, the problems that we think are interesting are highly nonlinear and nonequilibrium, and are very difficult to attack analytically, while the formal theoretical framework is now being firmly established. We stress that computer simulations can be a very important method for gaining insights into such tough but fascinating problems.

Though not adequately discussed in this paper, MD simulations under shear will become

increasingly important [22, 78, 79, 189, 190]. A new problem that we mention finally is nonlinear rheology in glass-forming liquids and polymers. MD simulations can be used to examine how glassy shear can affect glassy amorphous structures [45].

Acknowledgments

I have benefited from numerous discussions with many experimentalists and theorists. Among them, especial thanks are due to Kyozi Kawasaki, Masao Doi, D Beysens, W I Goldburg, Takeji Hashimoto, and Kenji Hamano. This review work was initiated a few years ago by kind encouragement of Hirohisa Endo and V Degiorgio.

Appendix A

We derive the reversible part of the stress tensor $\overleftrightarrow{\Pi}$ arising from the deviations of ϕ and $\overleftrightarrow{\mathbf{W}}$, neglecting dissipation for polymer solutions. We follow a method for near-critical fluids [191]. The velocity difference $\boldsymbol{w}$ between the polymer and the solvent will also be neglected. We consider a small fluid element at position $\boldsymbol{r}$ and at time t. Due to the velocity field $\boldsymbol{v}(\boldsymbol{r}, t)$, the element is displaced to a new position, $\boldsymbol{r}' = \boldsymbol{r} + \boldsymbol{u}$ with $\boldsymbol{u} = \boldsymbol{v}\,\delta t$, after a small time interval δt. Then the volume element $\mathrm{d}\boldsymbol{r}'$ is changed as follows:

$$\mathrm{d}\boldsymbol{r}' = \mathrm{d}\boldsymbol{r}\ (1 + \boldsymbol{\nabla}\cdot\boldsymbol{u}). \tag{A.1}$$

The composition ϕ is unchanged:

$$\phi'(\boldsymbol{r}') = \phi(\boldsymbol{r}). \tag{A.2}$$

The time dependence of $\phi(\boldsymbol{r}, t)$ and $\overleftrightarrow{\mathbf{W}}(\boldsymbol{r}, t)$ will be suppressed, for simplicity. The change of $\overleftrightarrow{\mathbf{W}}$ is calculated from (3.57) as follows:

$$W'_{ij}(\boldsymbol{r}') = W_{ij}(\boldsymbol{r}) + \sum_k (\tilde{D}_{ik} W_{kj} + W_{ik}\tilde{D}_{jk}) \tag{A.3}$$

where $\tilde{D}_{ij}$ is defined by

$$\tilde{D}_{ij} = \frac{\partial}{\partial x_j} u_{1i}. \tag{A.4}$$

Against these changes, the increment of $F\{\phi, \overleftrightarrow{\mathbf{W}}\}$ is expressed as

$$\delta F\{\phi, \overleftrightarrow{\mathbf{W}}\} = F'\{\phi', \overleftrightarrow{\mathbf{W}}'\} - F\{\phi, \overleftrightarrow{\mathbf{W}}\} = -\int \mathrm{d}\boldsymbol{r}\ \sum_{i,j} \Pi_{ij} \frac{\partial}{\partial x_j} u_i \tag{A.5}$$

which is simply the definition of Π_{ij}. The displaced free energy is written as

$$F'\{\phi', \overleftrightarrow{\mathbf{W}}'\} = \int \mathrm{d}\boldsymbol{r}'\ \left[f(\phi') + \frac{K(\phi')}{2} |\boldsymbol{\nabla}'\phi'|^2 + \frac{G(\phi')}{4} Q(\overleftrightarrow{\mathbf{W}}') \right]. \tag{A.6}$$

From $\boldsymbol{r}' = \boldsymbol{r} + \boldsymbol{u}$, the space derivatives are changed as follows:

$$\partial/\partial x'_i \cong \partial/\partial x_i - \sum_j (\partial u_j/\partial x_i)\ \partial/\partial x_j. \tag{A.7}$$

Using these relations, we obtain (3.59) and (3.60).

Appendix B

Here we show that the osmotic pressure $\pi(\phi, T)$ can be introduced using the original definition. Let a polymer solution in equilibrium (which is not deformed, and for which $\overleftrightarrow{\mathbf{W}} = \overleftrightarrow{\mathbf{I}}$) and a pure solvent be separated by a semi-permeable membrane through which solvent molecules can pass without resistance but polymer molecules are prohibited from passing because of their large sizes. Then there arises a pressure difference between the two regions, and the osmotic pressure $\pi(\phi, T)$ is dependent on the volume fraction ϕ of the polymer on the solution side. In our theory, equation (3.60) yields

$$\pi(\phi, T) = (\bar{\rho}/B)(\delta\rho - \delta\rho_0) - f \tag{B.1}$$

where $\delta\rho_0$ is the density deviation in the pure-solvent region. Because the solvent chemical potential μ_s in (3.63) is continuous through the membrane, we obtain $(\bar{\rho}/B)(\delta\rho - \delta\rho_0) = \phi\,\delta F/\delta\phi$, leading to

$$\pi(\phi, T) = \phi\,\partial f/\partial\phi - f \tag{B.2}$$

in accord with the expression in the literature [13]. The osmotic bulk modulus is then given by $K_{os} = \phi(\partial\pi/\partial\phi)_T$, leading to (3.52).

References

[1] Safran S A and Clark N A (ed) 1987 *Physics of Complex and Supermolecular Fluids* (New York: Wiley)
[2] Onuki A and Kawasaki K (ed) 1990 *Dynamics and Patterns in Complex Fluids* (Berlin: Springer)
[3] Sirota E B, Weitz D, Witten T and Israelachvili J (ed) 1992 *Complex Fluids* (Pittsburgh, PA: Materials Research Society)
[4] Silberberg A and Kuhn W 1954 *J. Polym. Sci.* **13** 21
[5] Lodge A S 1961 *Polymer* **2** 195
[6] Peterlin A and Turner D T 1965 *J. Polym. Sci., Polym. Lett.* **3** 517
[7] Utracki L A 1990 *Polymer Alloys and Blends. Thermodynamics and Rheology* (Munich: Hanser)
[8] Larson R G 1992 *Rheol. Acta* **31** 497
[9] Kawasaki K 1975 *Phase Transitions and Critical Phenomena* vol 5A, ed C Domb and J L Lebowitz (New York: Academic)
[10] Hohenberg P C and Halperin B I 1977 *Rev. Mod. Phys.* **49** 435
[11] Gunton D J, san Miguel M and Sahni P S 1983 *Phase Transitions and Critical Phenomena* vol 8, ed C Domb and J L Lebowitz (New York: Academic)
[12] Binder K 1991 *Phase Transformations of Materials (Materials Science and Technology 5)* ed P Haasen (Weinheim: VCH)
[13] de Gennes P G 1980 *Scaling Concepts in Polymer Physics* (Ithaca, NY: Cornell University Press)
[14] Doi M and Edwards S F 1986 *The Theory of Polymer Dynamics* (Oxford: Oxford University Press)
[15] Onuki A and Kawasaki K 1979 *Ann. Phys., NY* **121** 456
Onuki A and Kawasaki K 1980 *Prog. Theor. Phys. Suppl.* **69** 146
Onuki A, Yamazaki K and Kawasaki K 1981 *Ann. Phys., NY* **131** 217
[16] Onuki A 1989 *Int. J. Thermophys.* **10** 293
Onuki A 1994 *J. Phys. C: Solid State Phys.* **6** 193
[17] Beysens D, Gbadamassi M and Boyer L 1979 *Phys. Rev. Lett.* **43** 1253
Beysens D and Gbadamassi M 1980 *Phys. Rev.* A **22** 2250
[18] Beysens D, Gbadamassi M and Moncef-Bouanz B 1983 *Phys. Rev.* A **28** 2491
[19] Perrot F, Chan C K and Beysens D 1989 *Europhys. Lett.* **91** 65
Chan C K, Perrot F and Beysens D 1991 *Phys. Rev.* A **43** 1826
Baumberger T, Perrot F and Beysens D 1991 *Physica* A **174** 31
[20] Clark N A and Ackerson B J 1980 *Phys. Rev. Lett.* **44** 1005
Ackerson B J and Clark N A 1984 *Phys. Rev.* A **30** 906
Chen L B, Zukoski C F, Ackerson B J, Hanley H J M, Straty G C, Barker J and Glinka C J 1992 *Phys. Rev. Lett.* **69** 688
[21] Dozier W D and Chaikin P M 1982 *J. Physique* **43** 843

[22] Stevens M J and Robbins M O 1993 *Phys. Rev.* E **48** 3778
Komatsugawa H and Nosé S 1995 *Phys. Rev.* E **51** 5944
[23] Cates M E 1996 *J. Phys.: Condens. Matter* **8** 9167
[24] Diat O, Roux D and Nallet F 1993 *J. Physique* II **3** 1427
Sierro P and Roux D 1997 *Phys. Rev. Lett.* **78** 1496
[25] Berret J F, Roux R C, Porte G and Lindner P 1994 *Europhys. Lett.* **25** 521
Porte G, Berret J F and Harden J L 1997 *J. Physique* II **7** 459
Berret J F, Porte G and Decruppe J P 1997 *Phys. Rev.* E **55** 1668
[26] Yamamoto J and Tanaka H 1996 *Phys. Rev. Lett.* **74** 932
[27] Dhont J K G and Verduin H 1994 *J. Chem. Phys.* **101** 6193
Verduin H and Dhont J K G 1995 *Phys. Rev.* E **52** 1811
Dhont J K G and Verduin H 1997 *Physica* A **235** 87
[28] de Gennes P G 1976 *Mol. Cryst. Liq. Cryst.* **34** 91
[29] Bruinsma R F and Safinia C R 1991 *Phys. Rev.* A **43** 5377
Bruinsma R F and Rabin Y 1992 *Phys. Rev.* A **45** 994
[30] Olmsted P D and Goldbart P M 1992 *Phys. Rev.* A **46** 4966
[31] Spenley N A, Cates M E and McLeish T C B 1993 *Phys. Rev. Lett.* **71** 939
Decruppe J P, Capplelaere E and Cressely R 1997 *J. Physique* II **7** 257
[32] Fredrickson G H 1986 *J. Chem. Phys.* **85** 5306
Fredrickson G H and Larson R G 1987 *J. Chem. Phys.* **86** 1553
[33] Onuki A 1987 *J. Chem. Phys.* **87** 3692
[34] Cates M E and Milner S T 1989 *Phys. Rev. Lett.* **62** 1856
[35] Koppi K A, Tirrell M, Bates F S, Almdal K and Colby R H 1992 *J. Physique* II **2** 1941
Koppi K A, Tirrell M and Bates F S 1993 *Phys. Rev. Lett.* **70** 1449
[36] Winter H H, Scott D B, Gronski W, Okamoto S and Hashimoto T 1993 *Macromolecules* **26** 7236
Winley K I, Patel S S, Larson L G and Watanabe H 1993 *Macromolecules* **26** 2542
Winley K I, Patel S S, Larson L G and Watanabe H 1993 *Macromolecules* **26** 4373
McConnell G A, Lin M Y and Gast A P 1995 *Macromolecules* **28** 6754
Gupta V K, Krishnamoorti R, Kornfield J A and Smith S D 1995 *Macromolecules* **29** 1359
Zhang Y and Wiesner U 1995 *J. Chem. Phys.* **103** 4784
[37] Marrucci G 1985 *Pure Appl. Chem.* **57** 1545
Larson R G and Doi M 1991 *J. Rheol.* **35** 539
[38] Halsey T C and Toor W 1990 *Phys. Rev. Lett.* **65** 2820
[39] Martin J E and Odinek J 1995 *Phys. Rev. Lett.* **75** 2827
[40] Williamson R B and Busse W F 1967 *J. Appl. Phys.* **38** 4187
[41] McHugh A J and Forrest E H 1975 *J. Macromol. Sci. Phys.* **11** 219
[42] Rehage H, Wunderlich I and Hoffmann H 1986 *Prog. Colloid Polym. Sci.* **72** 51
Liu C and Pine D J 1996 *Phys. Rev. Lett.* **77** 2121
[43] Cates M E and Turner M S 1990 *Europhys. Lett.* **11** 681
Bruinsma R, Gelbert W M and Ben-Shaul 1992 *J. Chem. Phys.* **96** 7710
[44] Simmons J H, Ochoa R, Simmons K D and Mills J J 1988 *J. Non-Cryst. Solids* **105** 313
[45] Yamamoto R and Onuki A 1997 *Preprint*
[46] Brochard F and de Gennes P G 1992 *Langmuir* **8** 3033
[47] Migler K B, Hervet H and Léger L 1992 *Phys. Rev. Lett.* **70** 219
[48] Karnis A, Goldsmith H and Mason S 1966 *J. Colloid Interface Sci.* **22** 41
[49] de Gennes P G 1979 *J. Physique* **40** 783
[50] Nozières P and Quemada D 1986 *Europhys. Lett.* **2** 129
[51] Israelachvili J N and McGuiggan P M 1988 *Science* **241** 795
[52] Hu H-W, Carson G A and Granick S 1991 *Phys. Rev. Lett.* **66** 2758
[53] Onuki A and Kawasaki K 1979 *Phys. Lett.* **72A** 233
[54] Ackerson B J and Clark N A 1981 *J. Physique* **42** 929
[55] Onuki A and Kawasaki K 1982 *Physica* A **11** 607
Onuki A and Doi M 1986 *J. Chem. Phys.* **85** 1190
[56] Chou Y C and Goldburg W I 1981 *Phys. Rev. Lett.* **47** 1155
Beysens D and Gbadamassi M 1981 *Phys. Rev. Lett.* **47** 846
Beysens D, Gastand R and Decruppe F 1984 *Phys. Rev.* A **30** 1145
[57] Lai J and Fuller G G 1995 *J. Rheol.* **39** 893
Lai J and Fuller G G 1995 *J. Rheol.* **40** 153

[58] Koga T and Kawasaki K 1993 *Physica* A **196** 389
Kawasaki K and Koga T 1993 *Physica* A **201** 115
[59] Fukuhara F, Hamano K, Kuwahara N, Sengers J V and Krall A H 1993 *Phys. Lett.* **176A** 344
[60] Hobbie E K, Hair D W, Nakatani A I and Han C C 1992 *Phys. Rev. Lett.* **69** 1951
[61] Hashimoto T, Takebe T and Suehiro S 1988 *J. Chem. Phys.* **88** 5874
[62] Takebe T, Sawaoka R and Hashimoto T 1989 *J. Chem. Phys.* **91** 4369
[63] Takebe T, Fujioka K, Sawaoka R and Hashimoto T 1990 *J. Chem. Phys.* **93** 5271
[64] Fujioka K, Takebe T and Hashimoto T 1993 *J. Chem. Phys.* **96** 717
[65] Hashimoto T, Takebe T and Asakawa K 1993 *Physica* A **194** 338
[66] Asakawa K and Hashimoto T 1996 *J. Chem. Phys.* **105** 5216
[67] Onuki A and Hashimoto T 1989 *Macromolecules* **22** 879
[68] Yu J-W, Douglas J F, Hobbie E K, Kim S and Han C C 1997 *Phys. Rev. Lett.* **78** 2664
[69] Douglas J F 1992 *Macromolecules* **25** 1468
[70] Katsaros J D, Malone M F and Winter H H 1989 *Polym. Eng. Sci.* **29** 1434
Mani S, Malone M F and Winter H H 1992 *Macromolecules* **25** 5671
[71] Wu R-J, Shaw M T and Weiss R A 1992 *J. Rheol.* **36** 1605
[72] Chen Z J, Wu R-J, Shaw M T, Weiss R A, Fernandez M L and Higgins J S 1995 *Polym. Eng. Sci.* **35** 92
Fernandez M L, Higgins J S, Horst R and Wolf B A 1995 *Polymer* **36** 149
[73] Beysens D and Perrot F 1994 *J. Physique Lett.* **45** L31
[74] Imaeda T, Onuki A and Kawasaki K 1984 *Prog. Theor. Phys.* **71** 16
[75] Chan C K and Lin L 1990 *Europhys. Lett.* **11** 13
[76] Ohta T, Nozaki H and Doi M 1990 *J. Chem. Phys.* **93** 2664
[77] Rothman D H 1991 *Europhys. Lett.* **14** 337
[78] Butler B D, Hanley H J M, Hansen D and Evans D J 1996 *Phys. Rev.* B **53** 2450
[79] Padilla P and Toxvaerd S 1997 *J. Chem. Phys.* **106** 2342
[80] Furukawa H 1994 *Physica* A **204** 237
[81] Onuki A 1986 *Phys. Rev.* A **34** 3528
[82] Hashimoto T, Matsuzaka K, Moses E and Onuki A 1995 *Phys. Rev. Lett.* **74** 126
[83] Hobbie E K, Kim S and Han C C 1996 *Phys. Rev.* E **54** R5909
[84] Hamano K 1997 unpublished
[85] van Dijk M A, Eleveld M B and van Veelen A 1992 *Macromolecules* **25** 2274
Chen Z J, Shaw M T and Weiss R A 1995 *Macromolecules* **28** 2274
[86] Tomotika S 1932 *Proc. R. Soc.* A **150** 322
[87] Siggia E D 1979 *Phys. Rev.* A **20** 595
[88] Krall A H, Sengers J V and Hamano K 1993 *Phys. Rev.* E **48** 357
[89] Doi M and Ohta T 1991 *J. Chem. Phys.* **95** 1242
[90] Joshua M, Goldburg W I and Onuki A 1985 *Phys. Rev. Lett.* **54** 1175
Joshua M and Goldburg W I 1985 *Phys. Rev.* A **31** 3857
[91] Taylor G I 1934 *Proc. R. Soc.* A **146** 501
[92] Rallison J M 1984 *Annu. Rev. Fluid Mech.* **16** 46
[93] Hinch E J and Acrivos A 1980 *J. Fluid Mech.* **98** 305
Acrivos A 1988 *Physicochemical Hydrodynamics, Interfacial Phenomena* ed M G Velarde (New York: Plenum)
[94] Onuki A and Takesue S 1986 *Phys. Lett.* **114A** 133
[95] Min K Y, Stavans J, Piazza R and Goldburg W I 1989 *Phys. Rev. Lett.* **63** 1070
[96] Eswar N 1992 *Phys. Rev. Lett.* **68** 186
[97] Min K Y and Goldburg W I 1993 *Phys. Rev. Lett.* **70** 469
Min K Y and Goldburg W I 1993 *Phys. Rev. Lett.* **71** 569
Min K Y and Goldburg W I 1994 *Physica* A **204** 246
[98] Smoluchowski V 1917 *Z. Phys. Chem.* **92** 129
[99] Levich V G 1962 *Physicochemical Hydrodynamics* (Englewood Cliffs, NJ: Prentice-Hall)
[100] Alder P M 1981 *J. Colloid Interface Sci.* **83** 106
[101] Wang H, Zinchenko A Z and Davis R H 1994 *J. Fluid Mech.* **265** 161
[102] Swift D J and Friedlander S K 1964 *J. Colloid Sci.* **19** 621
[103] Doi M and Chen D 1989 *J. Chem. Phys.* **90** 5271
[104] West A H, Melrose and Ball R C 1994 *Phys. Rev.* E **49** 4237
[105] Roland C M and Böhm G G A 1984 *J. Polym. Sci., Polym. Phys. Edn* **22** 79
[106] Milner S T and Xi H 1996 *J. Rheol.* **40** 663

[107] Baumberger T, Perrot F and Beysens D 1992 *Phys. Rev.* A **46** 7636
[108] Batchelor G K 1979 *J. Fluid Mech.* **95** 369
[109] Kurdyumov V N and Polyamin A D 1990 *Fluid Dyn. (USSR)* **4** 611
[110] Lifshitz I M and Slyozov V V 1961 *J. Phys. Chem. Solids* **19** 35
[111] Oxtoby D W 1975 *J. Chem. Phys.* **62** 1463
Oxtoby D W and Metiu H 1976 *Phys. Rev. Lett.* **36** 1092
[112] Onuki A and Kawasaki K 1980 *Phys. Lett.* **75A** 485
[113] Onuki A 1987 *Phys. Rev.* A **35** 5149
[114] Felderhof B U 1970 *Physica* **48** 541
[115] Hamano K, Yamashita S and Sengers J V 1992 *Phys. Rev. Lett.* **68** 3578
[116] Batchelor G K 1970 *J. Fluid Mech.* **410** 545
[117] Doi M 1987 *Physics of Complex and Supermolecular Fluids* ed S A Safran and N A Clark (New York: Wiley) p 611
[118] Onuki A 1994 *Europhys. Lett.* **28** 175
[119] Hamano K, Ishi T, Ozawa M, Sengers J V and Krall A H 1995 *Phys. Rev.* E **51** 1254
[120] Takahashi Y, Kawashima N, Noda I and Doi M 1994 *J. Rheol.* **38** 699
Takahashi Y, Suzuki H, Nakagawa Y and Noda I 1994 *Macromolecules* **27** 6476
[121] Vinckier I, Moldenauers P and Mewis J 1996 *J. Rheol.* **40** 613
[122] Läuger J, Laubner C and Gronski W 1995 *Phys. Rev. Lett.* **75** 3576
[123] Jordhano G M, Mason J A and Sperling L H 1986 *Polym. Eng. Sci.* **26** 517
Miles I S and Zurek A 1988 *Polym. Eng. Sci.* **28** 796
[124] Emanuele A and Palma-Vittorelli M B 1992 *Phys. Rev. Lett.* **69** 81
[125] Bondár I and Dhont J K G 1996 *Phys. Rev. Lett.* **77** 5304
[126] Cametti C, Codastefano P, D'Arrigo G, Tartaglia P, Rouch J and Chen S H 1990 *Phys. Rev.* A **42** 3421
[127] Chashkin Yu R, Voronel A V, Smirnov V A and Gobunova V G 1979 *Sov. Phys.–JETP* **25** 79
[128] Onuki A 1990 *Prog. Theor. Phys. Suppl.* **99** 382
[129] Cannell D S 1975 *Phys. Rev.* A **12** 225
[130] Pine D J, Eswar N, Maher J V and Goldburg W I 1984 *Phys. Rev.* A **29** 308
[131] Onuki A 1984 *Phys. Lett.* **101A** 286
[132] Chan C K and Goldburg W I 1987 *Phys. Rev.* A **35** 1756
[133] Tong P, Goldburg W I, Stavans J and Onuki A 1989 *Phys. Rev. Lett.* **62** 2472
[134] Kolmogorov A N 1949 *Dokl. Akad. Nauk* **66** 825
[135] Lacasta A M, Sancho J M and Saguès S 1995 *Phys. Rev. Lett.* **75** 1791
[136] Atabaev O M, Saidov A A, Tadzhibaev P A, Tursumov Sh O and Khabibullaev P K 1990 *Dokl. Akad. Nauk* **315** 889
Khabibullaev P K, Butabaev M Sh, Pakharukov Yu V and Saidov A A 1991 *Dokl. Akad. Nauk* **320** 1372
Khabibullaev P K, Butabaev M Sh, Pakharukov Yu V and Saidov A A 1991 *Sov. Phys.–Dokl.* **36** 712
[137] Ver Strate G and Philippoff W 1974 *J. Polym. Sci., Polym. Lett.* **12** 267
[138] Rangel-Nafaile C, Metzner A B and Wissburn K F 1984 *Macromolecules* **17** 1187
[139] Krämer H and Wolf B A 1985 *Macromol. Chem. Rapid Commun.* **6** 21
[140] Moldenauers P, Yanase H, Mewis J, Fuller G G, Lee C-S and Magda J J 1993 *Rheol. Acta* **32** 1
[141] Laufer Z, Jalink H L and Staverman A J 1973 *J. Polym. Sci., Polym. Chem. Edn* **11** 3005
[142] Wu X L, Pine D J and Dixon P K 1991 *Phys. Rev. Lett.* **68** 2408
[143] Hashimoto T and Fujioka K 1991 *J. Phys. Soc. Japan* **60** 356
Hashimoto T and Kume T 1992 *J. Phys. Soc. Japan* **61** 1839
Moses E, Kume T and Hashimoto T 1994 *Phys. Rev. Lett.* **72** 2037
Murase H, Kume T, Hashimoto T, Ohta Y and Mizukami T 1995 *Macromolecules* **28** 7724
[144] Kume T, Hattori T and Hashimoto T 1997 *Macromolecules* **30** 427
[145] van Egmond J, Werner D E and Fuller G G 1992 *J. Chem. Phys.* **96** 7742
van Egmond J and Fuller G 1993 *Macromolecules* **26** 7182
[146] Nakatani A I, Douglas J F, Ban Y-B and Han C C 1994 *J. Chem. Phys.* **100** 3224
[147] Boue F and Lindner P 1994 *Europhys. Lett.* **25** 421
[148] Migler K, Liu C and Pine D J 1996 *Macromolecules* **29** 1422
[149] Helfand E and Fredrickson H 1989 *Phys. Rev. Lett.* **62** 2468
[150] Onuki A 1989 *Phys. Rev. Lett.* **62** 2472
[151] Onuki A 1990 *J. Phys. Soc. Japan* **59** 3423
Onuki A 1990 *J. Phys. Soc. Japan* **59** 3427
[152] Doi M 1990 *Dynamics and Patterns in Complex Fluids* ed A Onuki and K Kawasaki (Berlin: Springer) p 100

[153] Doi M and Onuki A 1992 *J. Physique* II **2** 1631
[154] Milner S T 1993 *Phys. Rev.* E **48** 3874
[155] Ji H and Helfand E 1995 *Macromolecules* **28** 3869
[156] Onuki A, Yamamoto R and Taniguchi T 1997 *J. Physique* II **7** 295
Onuki A, Yamamoto R and Taniguchi T 1997 *Prog. Colloid Polym. Sci.* at press
[157] Mendes E, Lindner P, Buzier M, Boue F and Bastide J 1991 *Phys. Rev. Lett.* **66** 1595
Mendes E, Oeser R, Hayes C, Boue F and Bastide J 1996 *Macromolecules* **29** 5574
[158] Bastide J, Leibler L and Prost J 1990 *Macromolecules* **23** 1821
[159] Onuki A 1993 *J. Physique* II **2** 45
Onuki A 1993 *Responsive Gels: Volume Transitions I (Advances in Polymer Science 109)* ed K Dusek (Berlin: Springer) p 63
[160] Rabin Y and Panyukov S 1997 *Macromolecules* **30** 301
[161] Brochard F and de Gennes P G 1977 *Macromolecules* **10** 1157
Brochard F 1983 *J. Physique* **44** 39
[162] Adam M and Delsanti M 1985 *Macromolecules* **18** 1760
[163] Dixon P K, Pine D J and Wu X L 1992 *Phys. Rev. Lett.* **68** 2239
[164] Štěpánek P, Brown W and Hvidt S 1996 *Macromolecules* **29** 8888
[165] Onuki A 1994 *J. Non-Cryst. Solids* **172–174** 1151
[166] Onuki A and Taniguchi T 1997 *J. Chem. Phys.* **106** 5761
[167] Tanaka T, Hocker L O and Benedik G B 1973 *J. Chem. Phys.* **59** 5151
[168] Wittmann H P and Fredrickson G H 1994 *J. Physique* I **4** 1791
[169] Sun T, Balazs A C and Jasnow D 1997 *Phys. Rev.* E **55** 6344
[170] Adam M and Delsanti M 1984 *J. Physique* **45** 1513
[171] Takahashi Y, Isono Y, Noda I and Nagasawa M 1985 *Macromolecules* **18** 1002
[172] Brochard F and de Gennes P G 1983 *Physicochem. Hydrodyn.* **4** 313
[173] Schwahn D, Janssen S and Springer T 1992 *J. Chem. Phys.* **97** 8775
Müller G, Schwahn D, Eckerlebe H, Rieger J and Springer T 1996 *J. Chem. Phys.* **104** 5826
[174] Bird R B, Armstrong R C and Hassager O 1987 *Dynamics of Polymeric Liquids* 2nd edn, vol 2 (New York: Wiley)
[175] Larson R G 1986 *Constitutive Equations for Polymer Melts and Solutions* (Boston, MA: Butterworths)
[176] Schmitt V, Marques C M and Lequeux F 1995 *Phys. Rev.* E **52** 4009
[177] Tirrell M and Malone M F 1977 *J. Polym. Sci., Polym. Phys. Edn* **15** 1569
[178] Hoh C J, Hookham P and Leal L G 1994 *J. Fluid Mech.* **266** 1
[179] Onuki A 1994 *Physica* A **204** 499
[180] Marrucci G 1972 *Trans. Soc. Rheol.* **16** 321
[181] Horst R and Wolf B A 1993 *Macromolecules* **26** 5676
[182] Casas-Vazquez J, Criado-Sancho M and Jou D 1993 *Europhys. Lett.* **23** 469
Jou D, Casas-Vazquez J and Criado-Sancho M 1995 *Adv. Polym. Sci.* **120** 207
[183] Grmela M 1988 *Phys. Lett.* **130A** 81
[184] Beris A N and Edwards B J 1994 *Thermodynamics of Flowing Systems* (Oxford: Oxford University Press)
[185] Taniguchi T and Onuki A 1996 *Phys. Rev. Lett.* **77** 4910
[186] Onuki A 1997 *J. Phys. Soc. Japan* **66** 1836
[187] Wolf B A and Sezen M C 1977 *Macromolecules* **10** 1010
[188] Magda J J, Lee C-S, Muller S J and Larson R G 1993 *Macromolecules* **26** 1696
[189] Evans D J and Morriss G P 1990 *Statistical Mechanics of Nonequilibrium Liquids* (New York: Academic)
[190] Hess S, Kröger M, Loose W, Borgmeyer C P, Schramek R, Voigt H and Weider T 1996 *Monte Carlo and Molecular Dynamics of Condensed Matter Systems* ed K Binder and G Ciccotti (Boulogne: SIF)
[191] Onuki A 1997 *Phys. Rev.* E **55** 403